

A 3D radiative transfer framework: VI. PHOENIX/3D example applications

Peter H. Hauschildt¹ and E. Baron^{1,2,3}

¹ Hamburger Sternwarte, Gojenbergsweg 112, 21029 Hamburg, Germany; yeti@hs.uni-hamburg.de

² Homer L. Dodge Dept. of Physics and Astronomy, University of Oklahoma, 440 W. Brooks, Rm 100, Norman, OK 73019 USA; baron@ou.edu

³ Computational Research Division, Lawrence Berkeley National Laboratory, MS 50F-1650, 1 Cyclotron Rd, Berkeley, CA 94720-8139 USA

Received date Accepted date

ABSTRACT

Aims. We demonstrate the application of our 3D radiative transfer framework in the model atmosphere code PHOENIX for a number of spectrum synthesis calculations for very different conditions.

Methods. The 3DRT framework discussed in the previous papers of this series was added to our general-purpose model atmosphere code PHOENIX/1D and an extended 3D version PHOENIX/3D was created. The PHOENIX/3D code is parallelized via the MPI library using a hierarchical domain decomposition and displays very good strong scaling.

Results. We present the results of several test cases for widely different atmosphere conditions and compare the 3D calculations with equivalent 1D models to assess the internal accuracy of the 3D modeling. In addition, we show the results for a number of parameterized 3D structures.

Conclusions. With presently available computational resources it is possible to solve the full 3D radiative transfer (including scattering) problem with the same micro-physics as included in 1D modeling.

Key words. Radiative transfer – Scattering

1. Introduction

In a series of papers Hauschildt & Baron (2006); Baron & Hauschildt (2007); Hauschildt & Baron (2008, 2009); Baron, Hauschildt, & Chen (2009, hereafter: Papers I–V), we have described a framework for the solution of the radiative transfer equation in 3D systems (3DRT), including a detailed treatment of scattering in continua and lines with a non-local operator splitting method. These papers deal solely with the radiation transport problem and its numerical solution for test cases designed to stress-test the algorithms and codes. It is important, however, to apply the radiative transfer codes to ‘real’ problems, e.g., model atmosphere simulations and to compare the results to 1D equivalents. We have extended our general purpose model atmosphere code PHOENIX to use the 3DRT framework so that the new version of PHOENIX can calculate both 1D (PHOENIX/1D) and 3D (PHOENIX/3D) models and spectra. In this paper we will describe the implementation and the results of PHOENIX calculations comparing the results of 1D and 3D spectrum syntheses for different model parameters.

2. Method

In the following discussion we use notation of Papers I – V. The basic framework and the methods used for the formal solution and the solution of the scattering problem via non-local operator splitting are discussed in detail in these papers and will not be repeated here.

3. PHOENIX/3D implementation and micro-physics

We have implemented PHOENIX/3D to use as much as possible of the micro-physics of PHOENIX/1D. This applies to the ACES equation of state (Barman, in preparation), to the b-f and f-f opacities, to dust opacities, and to the line opacities (PHOENIX/3D is presently restricted to LTE population densities). This includes individual line profiles (Gauss profiles for weak lines and Voigt profiles for strong lines depending on user-selectable selection criteria) for atomic and molecular lines with the same physics that is implemented in PHOENIX/1D, so that the results of the opacity calculations are equal for the same physical conditions for the two modes of PHOENIX.

The important considerations of PHOENIX/3D implementation are memory and CPU time consumption. The memory requirements of PHOENIX/3D compared to PHOENIX/1D are mostly due to the much larger number of voxels in the 3D case (typically 10^6 voxels) compared to the 1D case (usually 64–128 layers). As the memory required to store (and to compute) physical data such as the partial pressures of close to 900 species or the opacities scales linearly with the number of cells (or layers in 1D), it is obvious that only very small tests can be run without using domain decomposition methods on large scale parallel supercomputers. The domain decomposition implementation of PHOENIX/3D distributes the task of solving (and storing) the equation of state data and the wavelength dependent opacities to sets of processes each with its private memory. This linearly (with number of processes used) reduces the

amount of memory and time required for these tasks. For 1024 processes, this reduces the memory requirements to just a few MB per process to store the full equation of state results. The 3DRT requires, in comparison, a total of about 450MB for the same problem (due to the storage requirements of the non-local Λ^* -operator). Including the storage required for the computation of the line opacities, this is still just about 0.5GB/process, which is small compared to the typically available 4-16GB/core (CPU) on modern parallel supercomputers. In order to fully utilize the available memory per core and to increase flexibility we have implemented a hierarchical scheme similar to the parallel PHOENIX/1D implementation discussed in Hauschildt et al. (1997) and in Baron & Hauschildt (1998) and to the 3DRT parallelization in Paper II: We use a number of ‘clusters’ of processes where every cluster works on a different wavelength. Each cluster internally uses (on its subset of processes) the domain decomposition discussed above and the 3DRT parallelizations discussed in Paper I. This scheme can be adjusted to (a) fit the problem in the memory available for each core and (b) to optimize overall performances (e.g., depending on the number of solid angle points for the 3DRT solution or the coordinate system used). In the calculations presented here, we typically use clusters with 256–1024 processes, the number of clusters is limited only by the number of available CPUs.

4. Results

We have calculated a number of test models to compare the results of PHOENIX/1D calculations with PHOENIX/3D results. This comparison can be used to adjust the parameters of the 3D calculations (number of voxels or solid angle points) to give an accuracy that is acceptable for a given investment in computer time. The models that we show here were taken from the latest PHOENIX/1D grid (in preparation) of model atmospheres. In all stellar models (1D and 3D) we have used the set of solar abundances given in Asplund, Grevesse, & Sauval (2005).

4.1. Stellar Models

We have computed synthetic spectra for stellar model atmospheres with the parameters $T_{\text{eff}} = 3000\text{K}$, $\log(g) = 5.0$ (M dwarf), $T_{\text{eff}} = 5700\text{K}$, $\log(g) = 4.5$ (solar type star) and $T_{\text{eff}} = 9000\text{K}$, $\log(g) = 4.5$ (A star). The PHOENIX/1D models were computed with the latest setup in the input physics, including the ACES equation of state and the latest version of the atomic and molecular line databases. The model structures were then used as inputs to PHOENIX/3D to calculate synthetic spectra with the same sampling rates as the spectra from the PHOENIX/1D calculations. In the PHOENIX/3D calculations we have used a 3D spherical coordinate system with $n_r = 129$, $n_{\theta_c} = 65$ and $n_{\phi_c} = 129$ points for a total of about 1M voxels. The calculations used (if not specified otherwise) 64^2 solid angle points. For each object we calculated synthetic spectra with PHOENIX/1D and PHOENIX/3D and compare the fluxes of the 1D spectra to the flux vectors of the 3D results. As in paper IV we can use the (θ_c, ϕ_c) components of the 3D flux vector in 3D spherical coordinates to estimate the internal accuracy of the solution (as the F_{θ_c} and F_{ϕ_c} components are zero for spherically symmetric configurations). Figures 1 to 7 show selected results

for the different models. In these cases, the error due to the number of solid angle points is about 3% and in all tests run the differences between the PHOENIX/1D fluxes and the F_r component of the PHOENIX/3D calculation is of the same order. The differences between the 1D and 3D calculations are within the accuracy set by the number of solid angles in the 3D model. In order to verify that the errors get smaller with larger number of solid angles (as shown in Paper IV for simple test cases), we have run test models with 256^2 angles. Three example plots are shown in Figs. 8 to 10 The results show clearly that the higher solid angle resolution reduces the errors in F_{θ_c} and F_{ϕ_c} considerably and also improves the comparison for F_r to the 1D result, as the higher internal accuracy due to more solid angle points also increases the internal accuracy of F_r . This also shows that in 3D radiative transfer calculations the spatial resolution is not the only factor governing the quality of the solution, the solid angle resolution may in fact be more important, depending on the coordinate system used and the details of the problem that is calculated a number of test models to compare the results of PHOENIX/1D calculations with PHOENIX/3D results. This comparison can be used to adjust the parameters of the 3D calculations (number of voxels or solid angle points) to give an accuracy that is acceptable for a given investment in computer time. The models that we show here were taken from the latest PHOENIX/1D grid (in preparation) of model atmospheres. In all stellar models (1D and 3D) we have used the set of solar abundances given in Asplund, Grevesse, & Sauval (2005). We have calculated a number of test models to compare the results of PHOENIX/1D calculations with PHOENIX/3D results. This comparison can be used to adjust the parameters of the 3D calculations (number of voxels or solid angle points) to give an accuracy that is acceptable for a given investment in computer time. The models that we show here were taken from the latest PHOENIX/1D grid (in preparation) of model atmospheres. In all stellar models (1D and 3D) we have used the set of solar abundances given in Asplund, Grevesse, & Sauval (2005). being considered.

4.2. Scaling

In order to investigate the strong scaling properties of PHOENIX/3D we have constructed a small test case for a M dwarf model with 1000 wavelength points in a 3D spherical coordinate system with $n_r = 129$, $n_{\theta_c} = 65$ and $n_{\phi_c} = 129$ points for a total of about 1M voxels and 64^2 solid angle points and ran the calculations with different configurations of the domain decomposition and different total numbers of processes. The total workload remains constant in these calculations, so this is a strong scaling test where the workload per CPU drops as the number of processes increase (in contrast to a weak scaling test where the workload per process remains constant). The results are given in Table 1. In this table, ‘n(MPI)’ is the total number of MPI processes used, ‘cluster size’ is the number of processes that collaboratively work on a single wavelength (spatial domain decomposition) and ‘n(cluster)’ is the number of such clusters, each working on a different wavelength (energy domain decomposition). The product ‘cluster size’ \times ‘n(cluster)’ is always equal to ‘n(MPI)’. The column ‘Comm’ gives the time spent in MPI communication to collect the opacities from the different processes before the 3DRT calculation starts. The com-

munication requirements of the 3DRT calculations are included in the 3DRT column. The columns ‘line opacity’ give the time in seconds and scaling efficiency for all line opacity calculations, respectively, The columns ‘total’ give the total time and scaling efficiency, respectively, of the overall time spent in the computation of the 3D spectrum, this time does not include (small) contributions from the EOS solution and the line selection procedures. In the largest cluster size of 512 processes each process only works on 8 solid angles, whereas in the smallest cluster size (128) each process works on 32 solid angles. The work per solid angle is not perfectly constant and the amount of communication increases linearly as more processes collaborate, therefore, the scaling efficiency drops if more than about 512 processes are used for this problem size (i.e., number of solid angles). The scaling efficiency for the overall problem is quite good, the optimal value is about 98%. The drop-off for cluster sizes of 512 (and more) is due to (a) the relatively small number of solid angles leading to very little work for each 3DRT process and relatively more internal communication time in the 3DRT and (b) the small effect of the communication related to the spatial domain decomposition. We could not test setups with more than (the maximum available) 2048 processes; however, the test case should scale to 256k processes (number of wavelength points times cluster size), although for such a setup the overheads for, e.g., the solution of the equation of state and the line selection would be very noticeable.

4.3. 3D hydro model of solar convection

For a test with a computed 3D structure, we use the same example snapshot structure from H-G. Ludwig (Caffau et al. 2007; Wedemeyer et al. 2004) of a radiation-hydrodynamical simulation of convection in the solar atmosphere as in Paper III. The radiation transport calculations were performed with a total of $141 \times 141 \times 151$ Cartesian grid points in x , y , and z , respectively, for a total of 3 002 031 voxels, the periodic boundary conditions are set in the (horizontal) x, y plane. The 3D radiative transport equation is solved for $n_\theta = 64$ and $n_\phi = 64$ solid angle points, so that a total of about 12×10^9 intensities are calculated for each 3DRT iteration and wavelength point. For the tests described here, we are only using the temperature–pressure structure of the hydro model and ignore the velocity field.

We show example results in Figs. 11 to 14 in terms of the x , y , and z components of the flux vectors of each outer boundary voxel. The F_z components are, in addition, compared to the 1D model for the G2V star with the parameters $T_{\text{eff}} = 5700\text{K}$, $\log(g) = 4.5$ (* symbols in the figures). The general shape of the 3D spectra compare well to the 1D solar type model, of course there are large variations across the horizontal plane. In the UV the differences are largest, a number of voxel flux vectors show strong line emission, whereas the radiative+convective equilibrium 1D model only shows absorption features. This is to be expected as the 3D simulation of convection gives significant temperature variations across the volume considered, in particular in the horizontal plane. These variations have considerable effect on the radiative transfer solution: The horizontal components of the flux vectors of each voxel compared to the length of the flux vector $F = |\mathbf{F}|$, F_x/F and F_y/F , show quite substantial variations for different wavelengths. The variations are

much larger for smaller wavelengths (e.g., in the UV), due to the larger temperature dependence of the source functions for smaller wavelengths which translates to larger horizontal flux components for small wavelengths compared to longer wavelengths.

The components of the flux vectors in the $x - y$ plane can be larger than the z component, strongly dependent on the wavelength and on the location of the voxel. This is illustrated in Figs. 15 – 22, which show the flowlines of the $x - y$ components of the flux vector at the surface. The flow distances are much larger at optical wavelengths than in the UV due to the larger UV opacities. The ‘pattern’ of the horizontal energy flow depends strongly on the wavelength, it is also significantly different in the cores of strong lines compared to the surrounding continuum. The horizontal heat exchange could have in turn noticeable effects on the gas flow pattern.

4.4. Supernovae

The modeling of supernova spectra is a very important application of PHOENIX/3D modeling as it is expected, and explosion models show, that supernova explosions are intrinsically 3D driven. For the calculations shown here we use the Lagrangian frame 3DRT in spherical 3D coordinates as discussed in paper V. The test model is a simplified model for a type II supernova atmosphere with a maximum expansion speed of about $0.13c$. The model is a simple uniform composition model with the density parameterized as $\rho \propto r^{-9}$, and a “photospheric velocity” of $v_0 = 7600 \text{ km s}^{-1}$, and a model temperature of $T_{\text{model}} = 17000 \text{ K}$. These conditions correspond roughly to those of SN 1999em seven days after explosion. In Fig. 23 we show the CMF spectrum of the PHOENIX/3D run compared to the corresponding PHOENIX/1D synthetic spectrum. Due to computer time limitations we could only run a relatively small 3D model with $n_r = 129$, $n_{\theta_c} = 33$ and $n_{\phi_c} = 65$ points and 128^2 solid angle points. The small angular resolution causes the scatter in the F_r plots and the errors in the F_{θ_c} and F_{ϕ_c} components. In general the agreement is acceptable for this test run, for a full scale 3D SN spectrum the resolution in (θ_c, ϕ_c) should be increased to $(65, 129)$ at least and the angular resolution should be at least 512^2 (which reduces the bandwidth dramatically, see Paper V).

5. Summary and Conclusions

We have described first results we have obtained by incorporating the 3D radiative transfer framework we have discussed in Papers I-V into our general purpose model atmosphere package PHOENIX, thus allowing both 1D models (PHOENIX/1D) and 3D models (PHOENIX/3D) with the same micro-physics. We have verified and tested PHOENIX/3D by computing a number of test spectra for 1D conditions and comparing the results to the corresponding PHOENIX/1D calculations. The conditions range from M dwarfs, solar type stars to A stars and Type II supernovae with relativistic expansion speeds. In addition, we have calculated spectra for a 3D hydrodynamical simulation of solar atmosphere convection. These tests demonstrate that it is now possible to calculate realistic spectra for 3D configurations including complex micro-physics. PHOENIX/3D can be used to calculate synthetic spectra for a number of complex 3D atmosphere model,

including irradiated stars or planets, novae, and supernovae. We are currently working on extensions of the 3D radiative transfer framework to arbitrary velocity fields in the Euler (for low velocities, e.g., in convection simulations or planetary winds) and the Lagrangian (for Supernovae, accretion disks and matter flow in the vicinity of black holes) frames, which will extend the applications of PHOENIX/3D significantly.

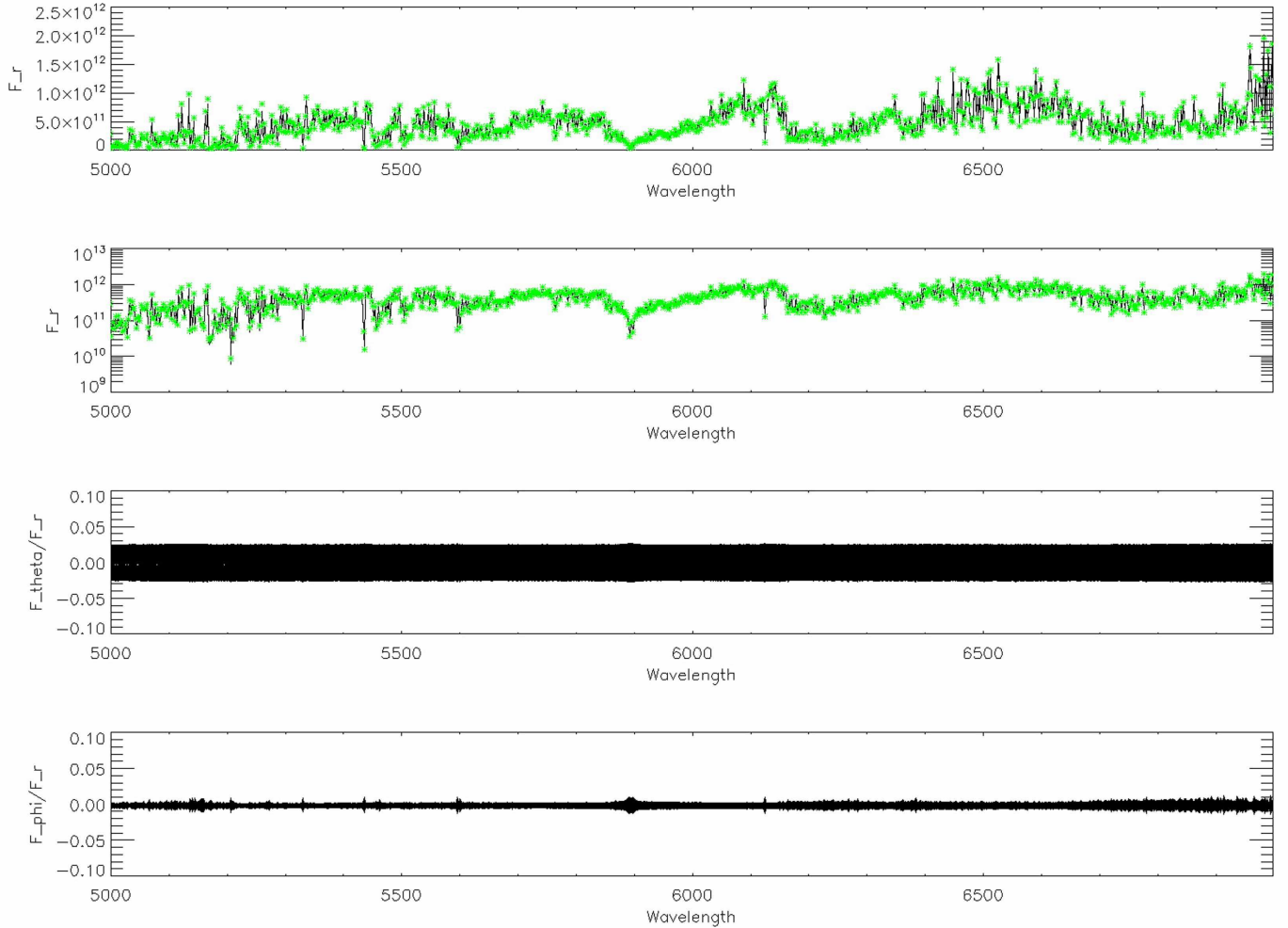
Acknowledgements. This work was supported in part by DFG GrK 1351 and SFB 676, as well as NSF grant AST-0707704, and US DOE Grant DE-FG02-07ER41517. The calculations presented here were performed at the Höchstleistungs Rechenzentrum Nord (HLRN); at the Hamburger Sternwarte IBM Regatta Systems, Apple G5, and Delta Opteron clusters financially supported by the DFG and the State of Hamburg; and at the National Energy Research Supercomputer Center (NERSC), which is supported by the Office of Science of the U.S. Department of Energy under Contract No. DE-AC03-76SF00098. We thank all these institutions for a generous allocation of computer time.

References

- Asplund, M., Grevesse, N., & Sauval, A. J. 2005, in ASP Conf. Ser. 336: Cosmic Abundances as Records of Stellar Evolution and Nucleosynthesis, ed. T. G. Barnes, III & F. N. Bash, 25
- Baron, E. & Hauschildt, P. H. 1998, ApJ, 495, 370
- Baron, E. & Hauschildt, P. H. 2007, A&A, 468, 255
- Baron, E., Hauschildt, P. H., & Chen, B. 2009, A&A, 498, 987
- Caffau, E., Steffen, M., Sbordone, L., Ludwig, H.-G., & Bonifacio, P. 2007, A&A, 473, L9
- Hauschildt, P. H. & Baron, E. 2006, A&A, 451, 273
- Hauschildt, P. H. & Baron, E. 2008, A&A, 490, 873
- Hauschildt, P. H. & Baron, E. 2009, A&A, 498, 981
- Hauschildt, P. H., Baron, E., & Allard, F. 1997, ApJ, 483, 390
- Wedemeyer, S., Freytag, B., Steffen, M., Ludwig, H.-G., & Holweger, H. 2004, A&A, 414, 1121

Table 1. Strong scaling behavior of a M dwarf model test case for different configurations and total number of processors used. See text for details.

n(MPI)	cluster size	n(cluster)	Timing:				Scaling:				
			line opacity	3DRT	Comm	total	Line opacity	3DRT	total		
2048	512	4	2473	9942	436	12909	96.7%	79.3%	81.9%		
2048	256	8	2414	8054	285	10789	99.1%	97.9%	98.0%		
1024	512	2	4900	20103	754	25872	97.6%	78.4%	81.7%		
1024	256	4	4741	15966	604	21385	100.9%	98.7%	98.9%		
1024	128	8	4681	14275	471	19483	102.2%	110.4%	108.6%		
512	512	1	9780	39793	1539	51341	97.8%	79.2%	82.4%		
512	256	2	9566	31524	1061	42300	100.0%	100.0%	100.0%		

**Fig. 1.** Comparison between the PHOENIX/1D optical spectrum and the flux vectors across the outermost voxels for the PHOENIX/3D spectra computed for the M dwarf test model ($T_{\text{eff}} = 3000\text{K}$, $\log(g) = 5.0$, ‘*’ symbols). In the PHOENIX/3D calculations we have used a 3D spherical coordinate system with $n_r = 129$, $n_\theta = 65$ and $n_\phi = 129$ points for a total of about 1M voxels. The calculations used 64^2 solid angle points. The top panels show the F_r component of all outer voxels in linear and logarithmic scales, respectively. The bottom panels show the corresponding runs of F_θ/F_r and F_ϕ/F_r , respectively. The should be identically zero and the deviations measure the internal accuracy. See Figs. 8 to 10 for high-accuracy solutions for comparison. The wavelengths are given in Å and the fluxes are in cgs units.

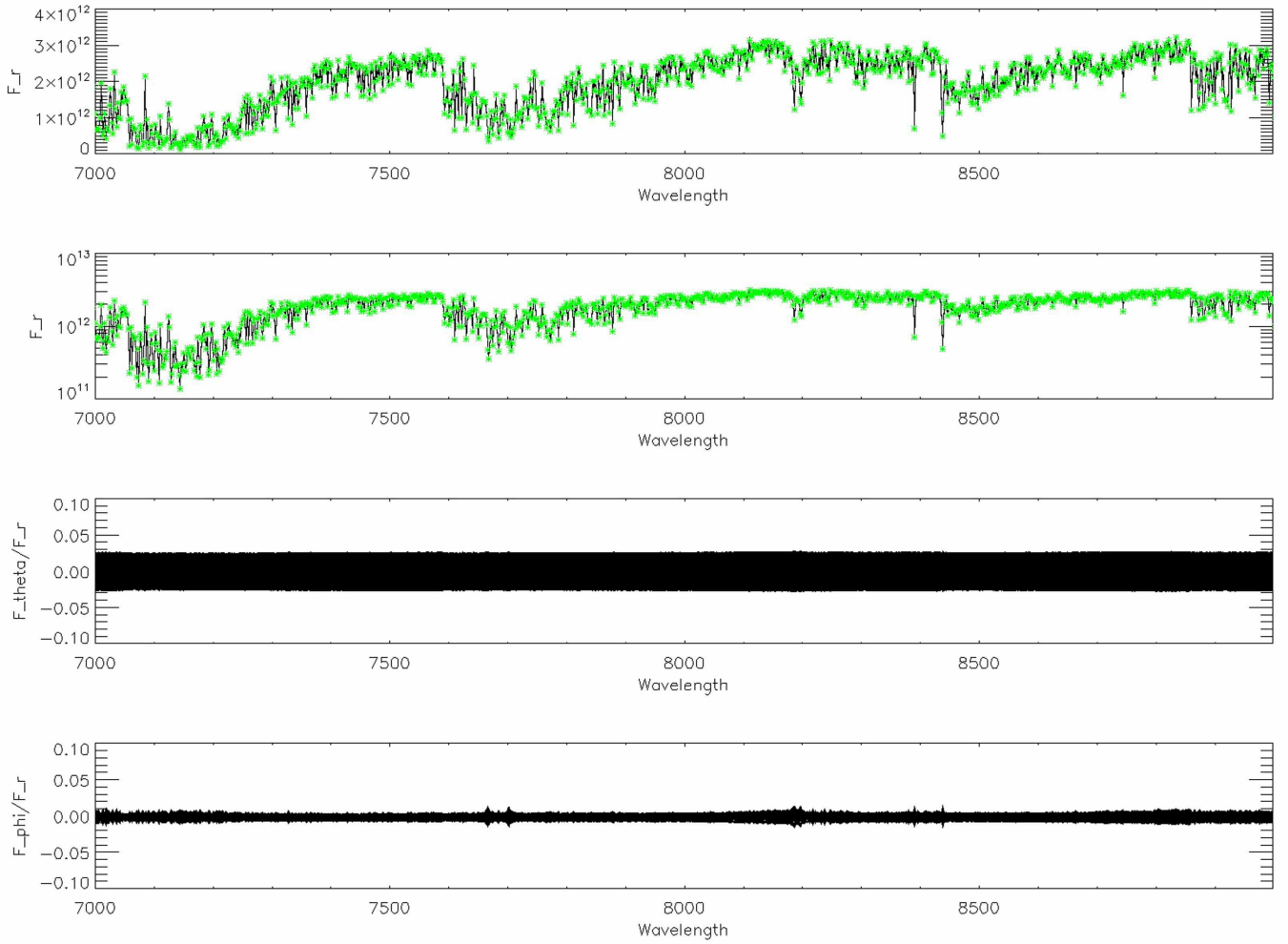


Fig. 2. Comparison between the PHOENIX/1D near infrared spectrum and the flux vectors across the outermost voxels for the PHOENIX/3D spectra computed for the M dwarf test model ($T_{\text{eff}} = 3000\text{K}$, $\log(g) = 5.0$, ‘*’ symbols). In the PHOENIX/3D calculations we have used a 3D spherical coordinate system with $n_r = 129$, $n_{\theta_c} = 65$ and $n_{\phi_c} = 129$ points for a total of about 1M voxels. The calculations used 64^2 solid angle points. The top panels show the F_r component of all outer voxels in linear and logarithmic scales, respectively. The bottom panels show the corresponding runs of F_{θ}/F_r and F_{ϕ}/F_r , respectively. The should be identically zero and the deviations measure the internal accuracy. See Figs. 8 and 10 for high-accuracy solutions for comparison. The wavelengths are given in \AA and the fluxes are in cgs units.

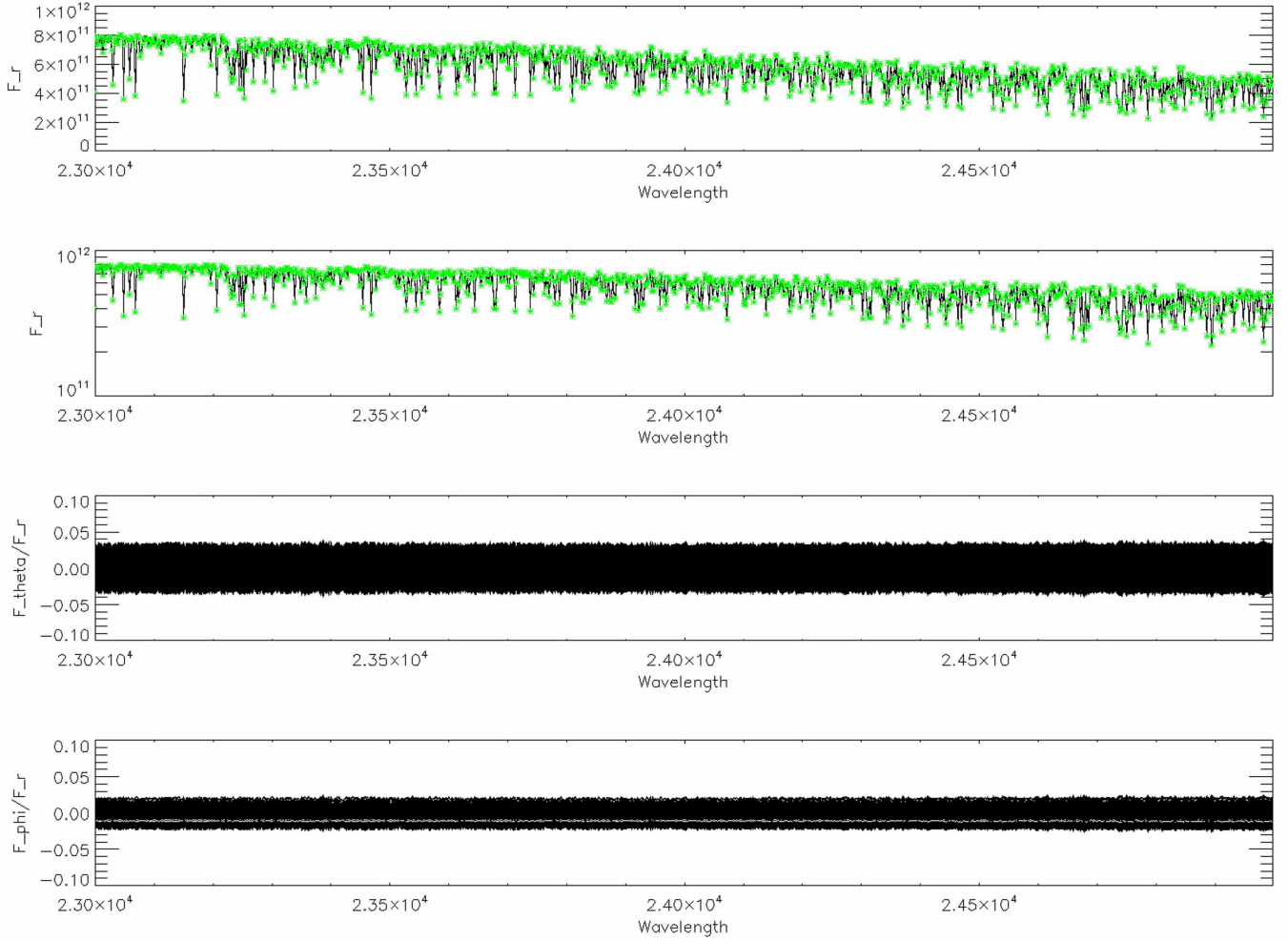


Fig. 3. Comparison between the PHOENIX/1D infrared spectrum and the flux vectors across the outermost voxels for the PHOENIX/3D spectra computed for the M dwarf test model ($T_{\text{eff}} = 3000\text{K}$, $\log(g) = 5.0$, ‘*’ symbols). In the PHOENIX/3D calculations we have used a 3D spherical coordinate system with $n_r = 129$, $n_{\theta_c} = 65$ and $n_{\phi_c} = 129$ points for a total of about 1M voxels. The calculations used 64^2 solid angle points. The top panels show the F_r component of all outer voxels in linear and logarithmic scales, respectively. The bottom panels show the corresponding runs of F_{θ}/F_r and F_{ϕ}/F_r , respectively. They should be identically zero and the deviations measure the internal accuracy. See Figs. 8 and 10 for high-accuracy solutions for comparison. The wavelengths are given in \AA and the fluxes are in cgs units.

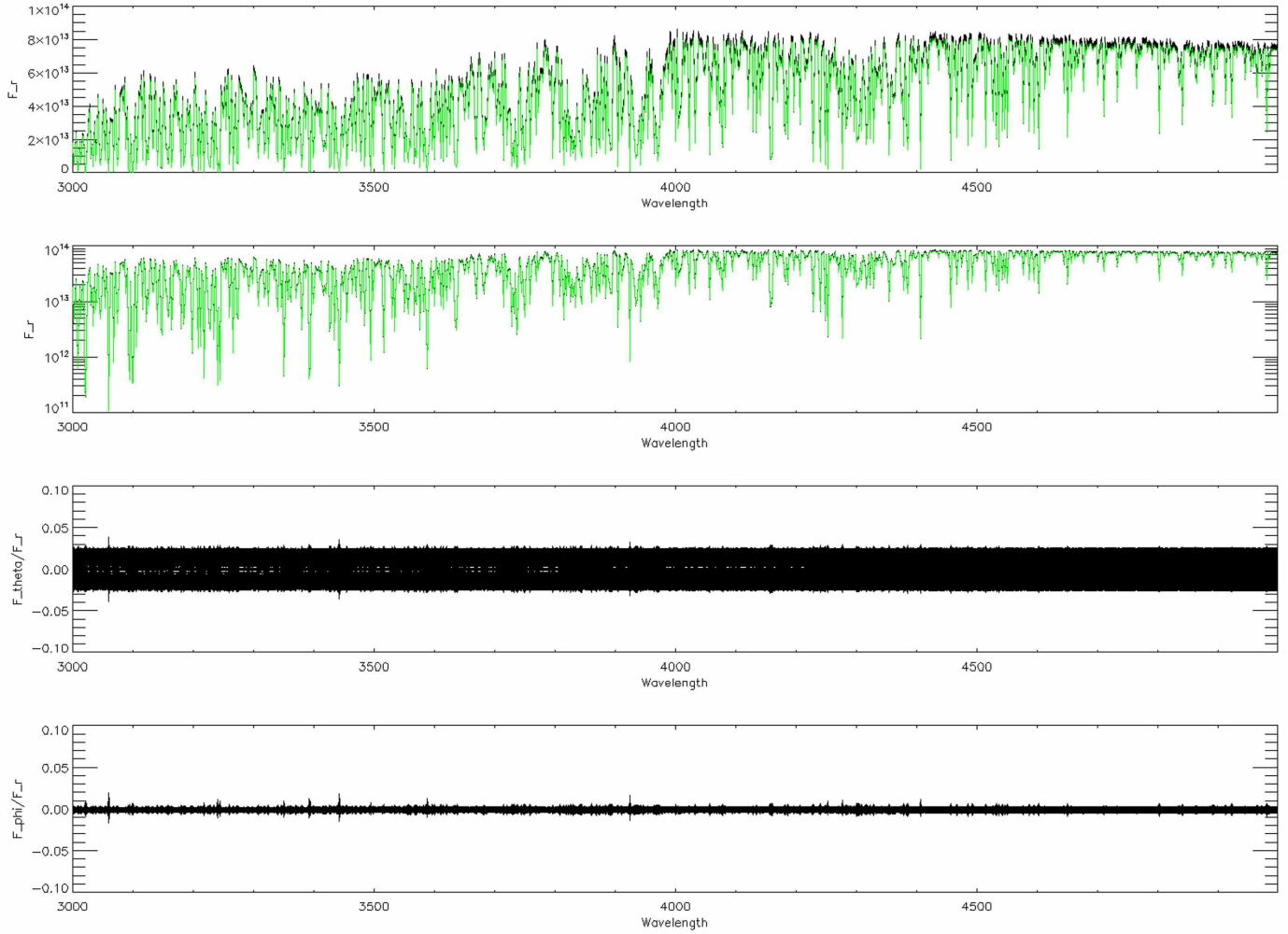


Fig. 4. Comparison between the PHOENIX/1D near UV spectrum and the flux vectors across the outermost voxels for the PHOENIX/3D spectra computed for the G2V dwarf test model ($T_{\text{eff}} = 5700\text{K}$, $\log(g) = 4.5$, ‘*’ symbols). In the PHOENIX/3D calculations we have used a 3D spherical coordinate system with $n_r = 129$, $n_{\theta_c} = 65$ and $n_{\phi_c} = 129$ points for a total of about 1M voxels. The calculations used 64^2 solid angle points. The top panels show the F_r component of all outer voxels in linear and logarithmic scales, respectively. The bottom panels show the corresponding runs of F_{θ}/F_r and F_{ϕ}/F_r , respectively. They should be identically zero and the deviations measure the internal accuracy. See Figs. 8 and 10 for high-accuracy solutions for comparison. The wavelengths are given in \AA and the fluxes are in cgs units.

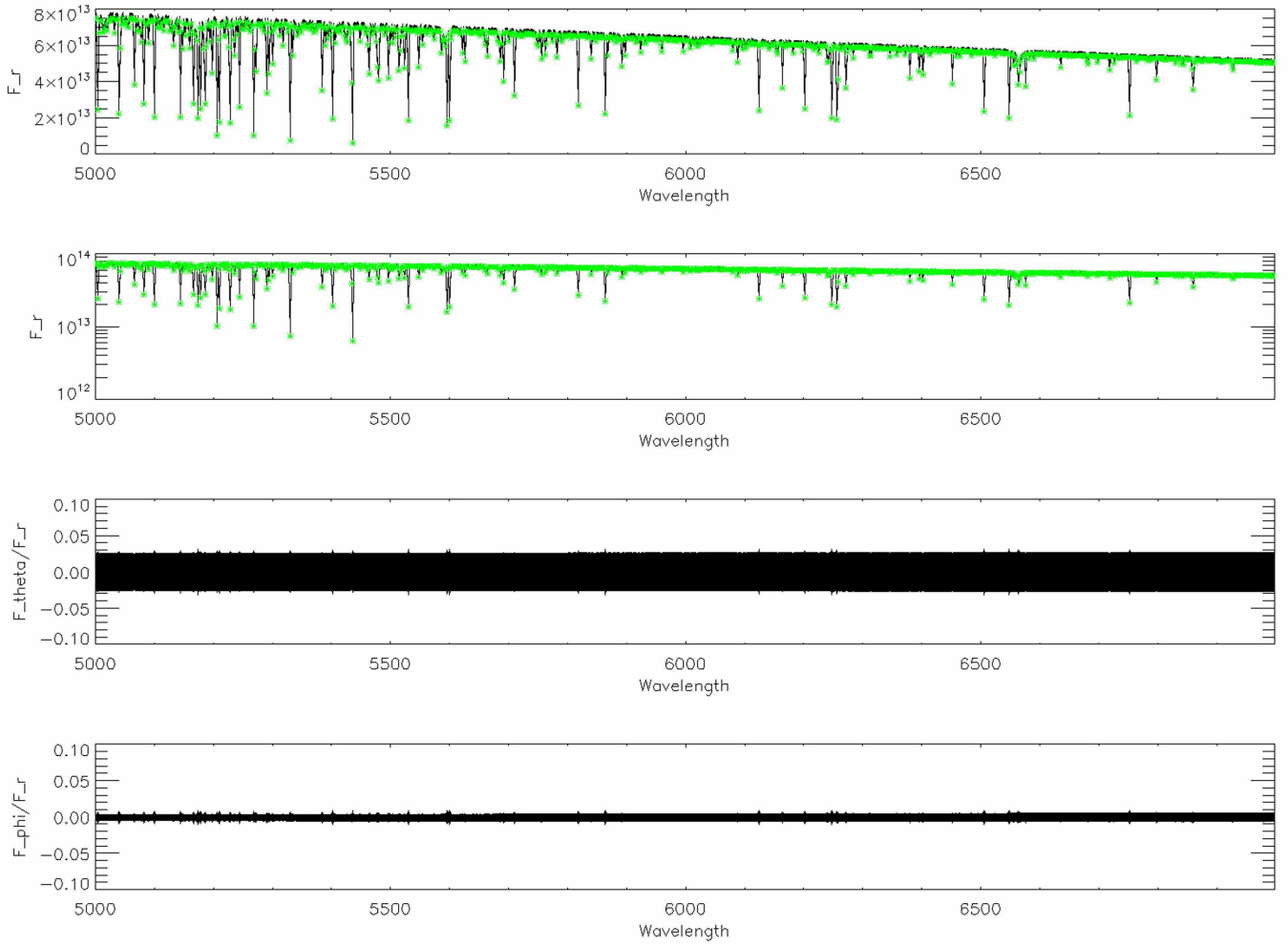


Fig. 5. Comparison between the PHOENIX/1D optical spectrum and the flux vectors across the outermost voxels for the PHOENIX/3D spectra computed for the G2V dwarf test model ($T_{\text{eff}} = 5700\text{K}$, $\log(g) = 4.5$, ‘*’ symbols). In the PHOENIX/3D calculations we have used a 3D spherical coordinate system with $n_r = 129$, $n_{\theta_c} = 65$ and $n_{\phi_c} = 129$ points for a total of about 1M voxels. The calculations used 64^2 solid angle points. The top panels show the F_r component of all outer voxels in linear and logarithmic scales, respectively. The bottom panels show the corresponding runs of F_{θ}/F_r and F_{ϕ}/F_r , respectively. The should be identically zero and the deviations measure the internal accuracy. See Figs. 8 and 10 for high-accuracy solutions for comparison. The wavelengths are given in \AA and the fluxes are in cgs units.

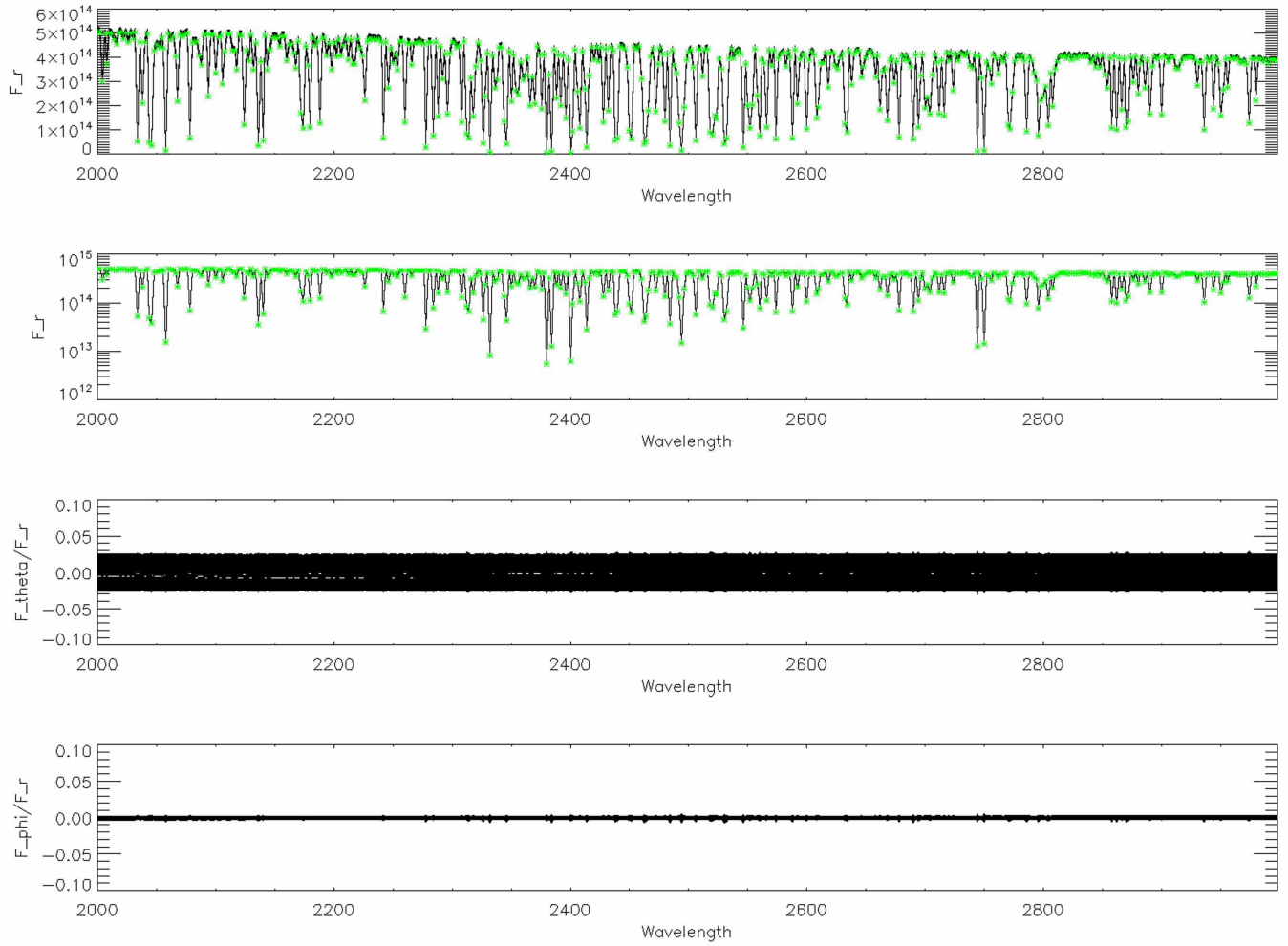


Fig. 6. Comparison between the PHOENIX/1D optical spectrum and the flux vectors across the outermost voxels for the PHOENIX/3D spectra computed for the A dwarf test model ($T_{\text{eff}} = 9000\text{K}$, $\log(g) = 4.5$, ‘*’ symbols). In the PHOENIX/3D calculations we have used a 3D spherical coordinate system with $n_r = 129$, $n_{\theta} = 65$ and $n_{\phi} = 129$ points for a total of about 1M voxels. The calculations used 64^2 solid angle points. The top panels show the F_r component of all outer voxels in linear and logarithmic scales, respectively. The bottom panels show the corresponding runs of F_{θ}/F_r and F_{ϕ}/F_r , respectively. They should be identically zero and the deviations measure the internal accuracy. See Figs. 8 and 10 for high-accuracy solutions for comparison. The wavelengths are given in Å and the fluxes are in cgs units.

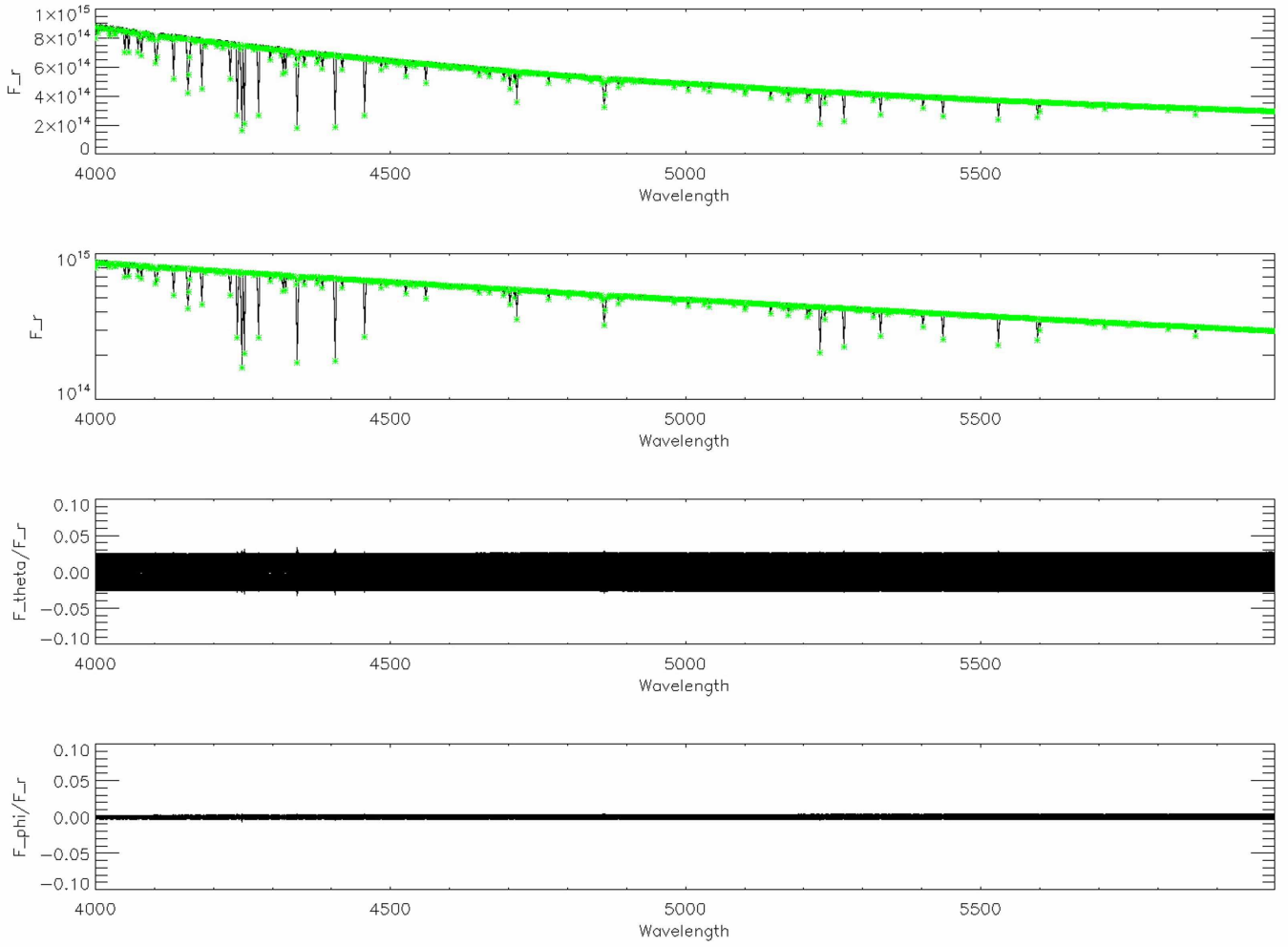


Fig. 7. Comparison between the PHOENIX/1D UV spectrum and the flux vectors across the outermost voxels for the PHOENIX/3D spectra computed for the A dwarf test model ($T_{\text{eff}} = 9000\text{K}$, $\log(g) = 4.5$, ‘*’ symbols). In the PHOENIX/3D calculations we have used a 3D spherical coordinate system with $n_r = 129$, $n_{\theta} = 65$ and $n_{\phi} = 129$ points for a total of about 1M voxels. The calculations used 64^2 solid angle points. The top panels show the F_r component of all outer voxels in linear and logarithmic scales, respectively. The bottom panels show the corresponding runs of F_{θ}/F_r and F_{ϕ}/F_r , respectively. They should be identically zero and the deviations measure the internal accuracy. See Figs. 8 and 10 for high-accuracy solutions for comparison. The wavelengths are given in Å and the fluxes are in cgs units.

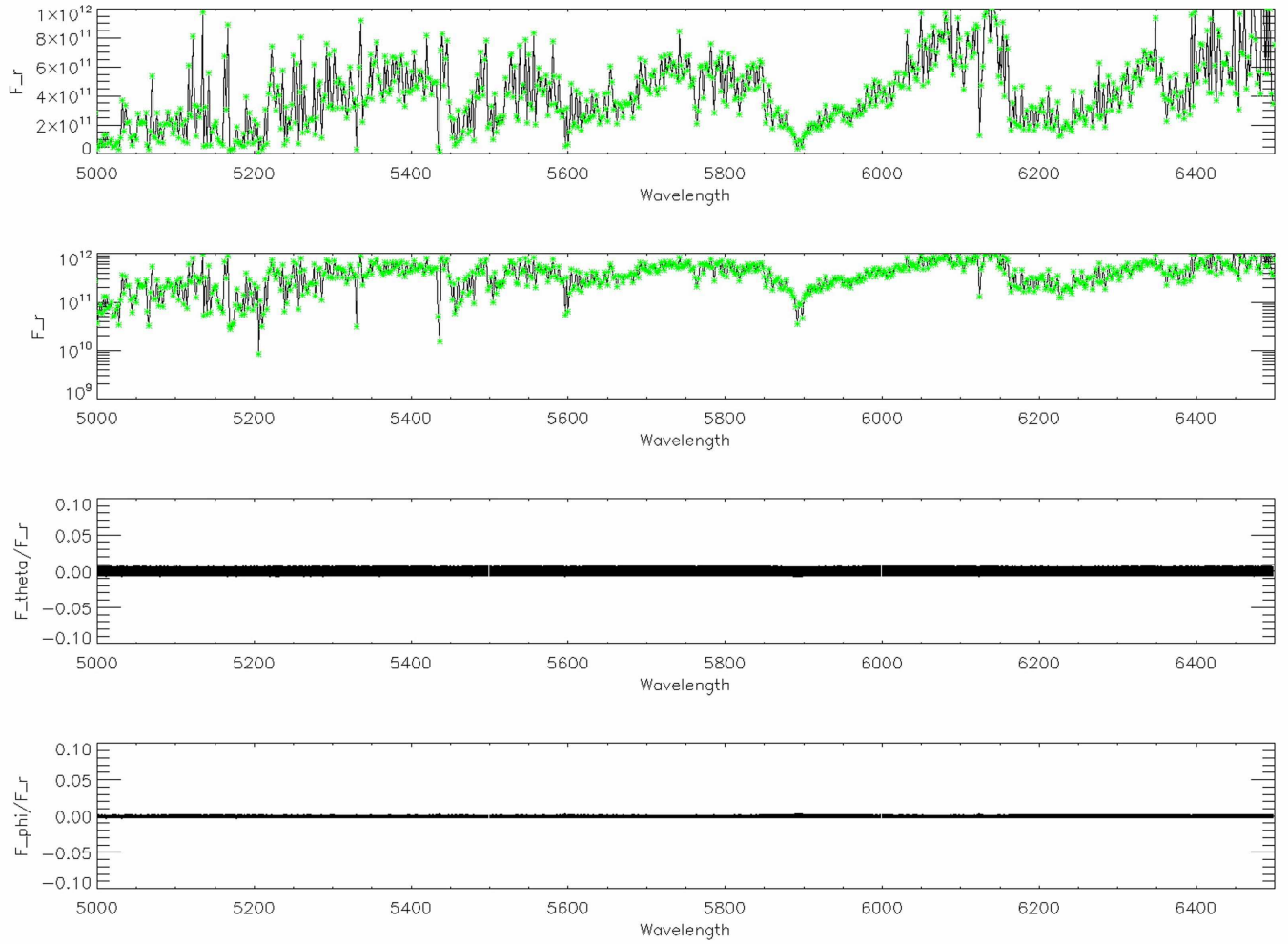


Fig. 8. Comparison between the PHOENIX/1D optical spectrum and the flux vectors across the outermost voxels for the higher resolution PHOENIX/3D spectra computed for the M dwarf test model ($T_{\text{eff}} = 3000\text{K}$, $\log(g) = 5.0$, ‘*’ symbols). In the PHOENIX/3D calculations we have used a 3D spherical coordinate system with $n_r = 129$, $n_{\theta_c} = 65$ and $n_{\phi_c} = 129$ points for a total of about 1M voxels. The calculations used 256^2 solid angle points. The top panels show the F_r component of all outer voxels in linear and logarithmic scales, respectively. The bottom panels show the corresponding runs of F_{θ}/F_r and F_{ϕ}/F_r , respectively. They should be identically zero and the deviations measure the internal accuracy. The wavelengths are given in \AA and the fluxes are in cgs units.

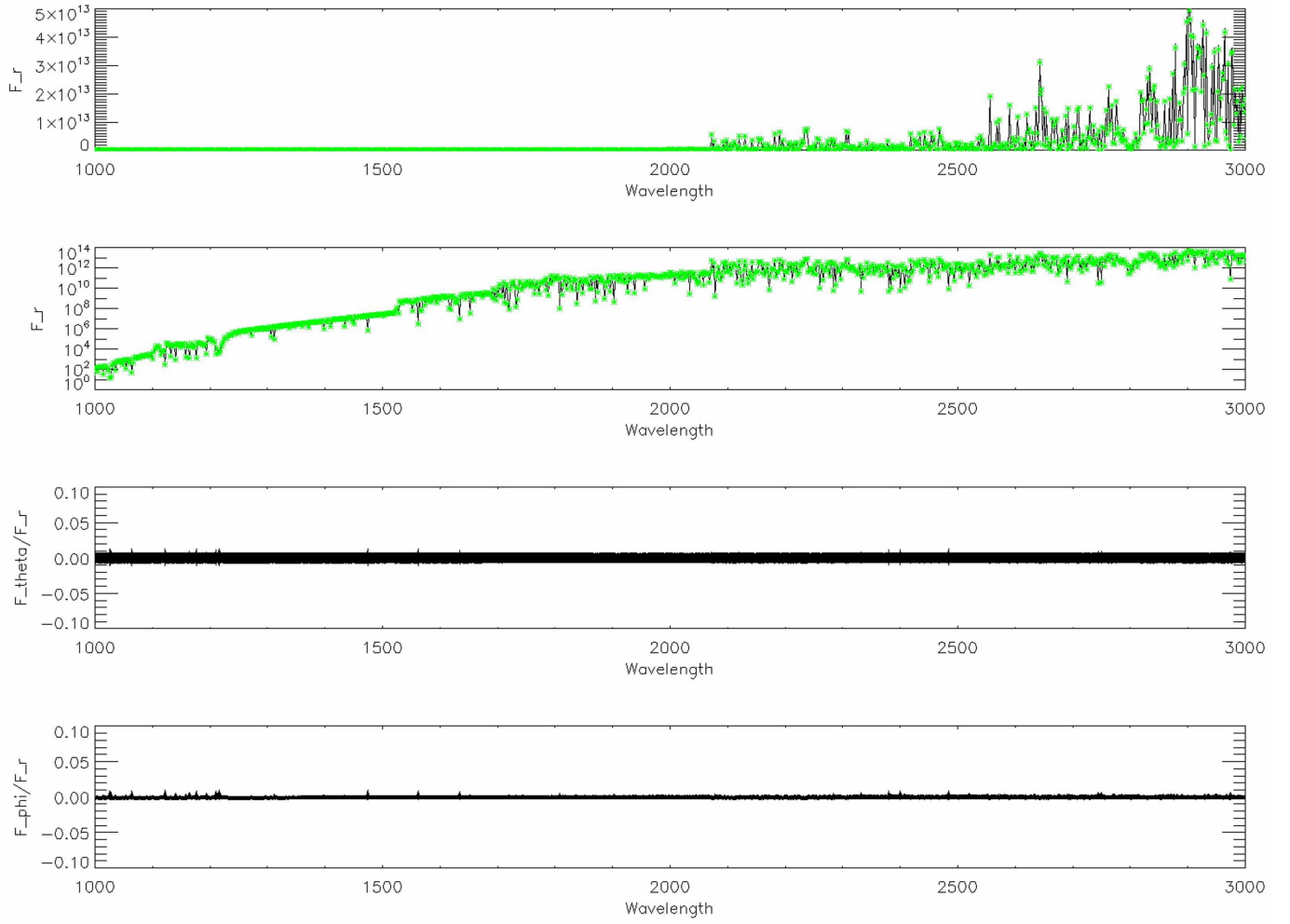


Fig. 9. Comparison between the PHOENIX/1D UV spectrum and the flux vectors across the outermost voxels for the higher resolution PHOENIX/3D spectra computed for the G2V dwarf test model ($T_{\text{eff}} = 5700\text{K}$, $\log(g) = 4.5$, ‘*’ symbols). In the PHOENIX/3D calculations we have used a 3D spherical coordinate system with $n_r = 129$, $n_{\theta_c} = 65$ and $n_{\phi_c} = 129$ points for a total of about 1M voxels. The calculations used 256^2 solid angle points. The top panels show the F_r component of all outer voxels in linear and logarithmic scales, respectively. The bottom panels show the corresponding runs of F_{θ}/F_r and F_{ϕ}/F_r , respectively. They should be identically zero and the deviations measure the internal accuracy. The wavelengths are given in Å and the fluxes are in cgs units.

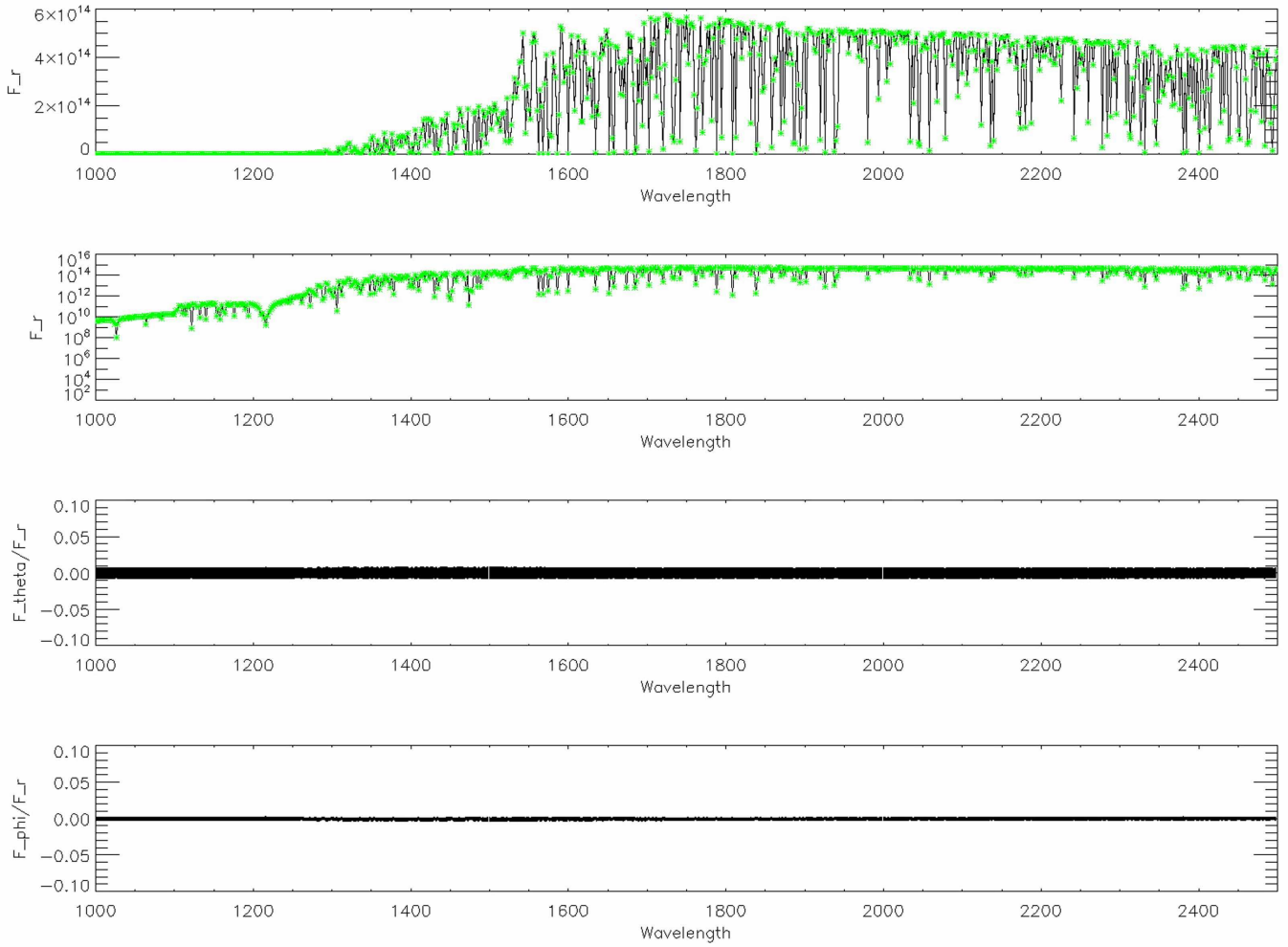


Fig. 10. Comparison between the optical PHOENIX/1D spectrum and the flux vectors across the outermost voxels for the higher resolution PHOENIX/3D spectra computed for the A dwarf test model ($T_{\text{eff}} = 5700\text{K}$, $\log(g) = 4.5$, ‘*’ symbols). In the PHOENIX/3D calculations we have used a 3D spherical coordinate system with $n_r = 129$, $n_{\theta_c} = 65$ and $n_{\phi_c} = 129$ points for a total of about 1M voxels. The calculations used 256^2 solid angle points. The top panels show the F_r component of all outer voxels in linear and logarithmic scales, respectively. The bottom panels show the corresponding runs of F_{θ}/F_r and F_{ϕ}/F_r , respectively. They should be identically zero and the deviations measure the internal accuracy. The wavelengths are given in Å and the fluxes are in cgs units.

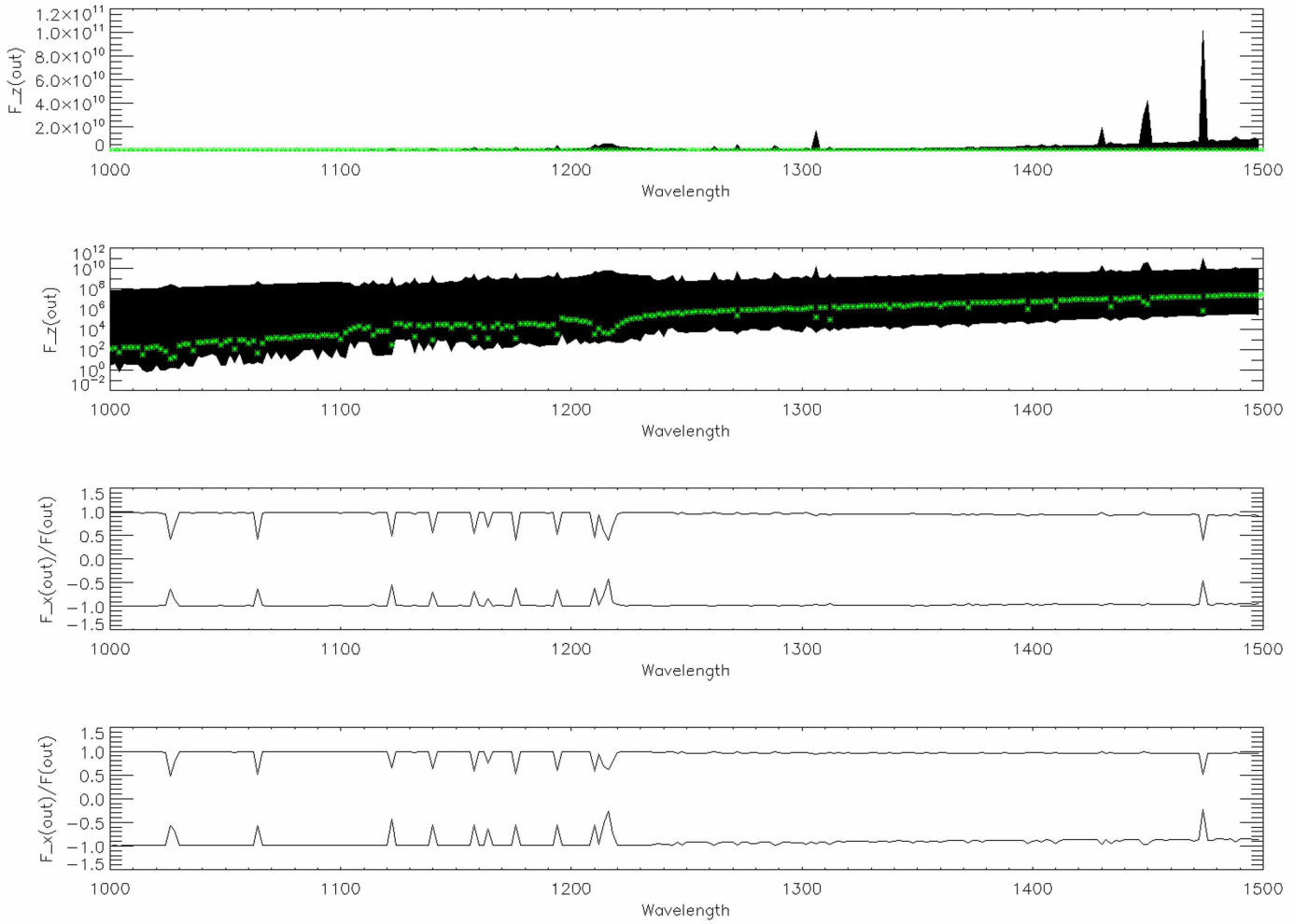


Fig. 11. Comparison between the flux vectors across the outermost voxels for the PHOENIX/3D UV spectra computed for the 3D hydro structure and the PHOENIX/1D spectrum for the G2V dwarf test model ($T_{\text{eff}} = 5700\text{K}$, $\log(g) = 4.5$). In the PHOENIX/3D calculations we have used a 3D coordinate system with a total of $141 \times 141 \times 151$ Cartesian grid points in x , y , and z , respectively, the periodic boundary conditions are set in the (horizontal) x , y plane. The 3D radiative transport equation is solved for $n_{\theta} = 64$ and $n_{\phi} = 64$ solid angle points. The top panels show the F_z component of all outer voxels in linear and logarithmic scales, respectively, compared to the results of the 1D comparison model. The bottom panels show the corresponding maxima and minima of $F_x/|\mathbf{F}|$ and $F_y/|\mathbf{F}|$, respectively, over all surface voxels for each wavelength. These panels show that in the 3D structure even at the surface a substantial horizontal energy flow takes place, see also figures 15 – 22. See text for details. The wavelengths are given in \AA and the fluxes are in cgs units.

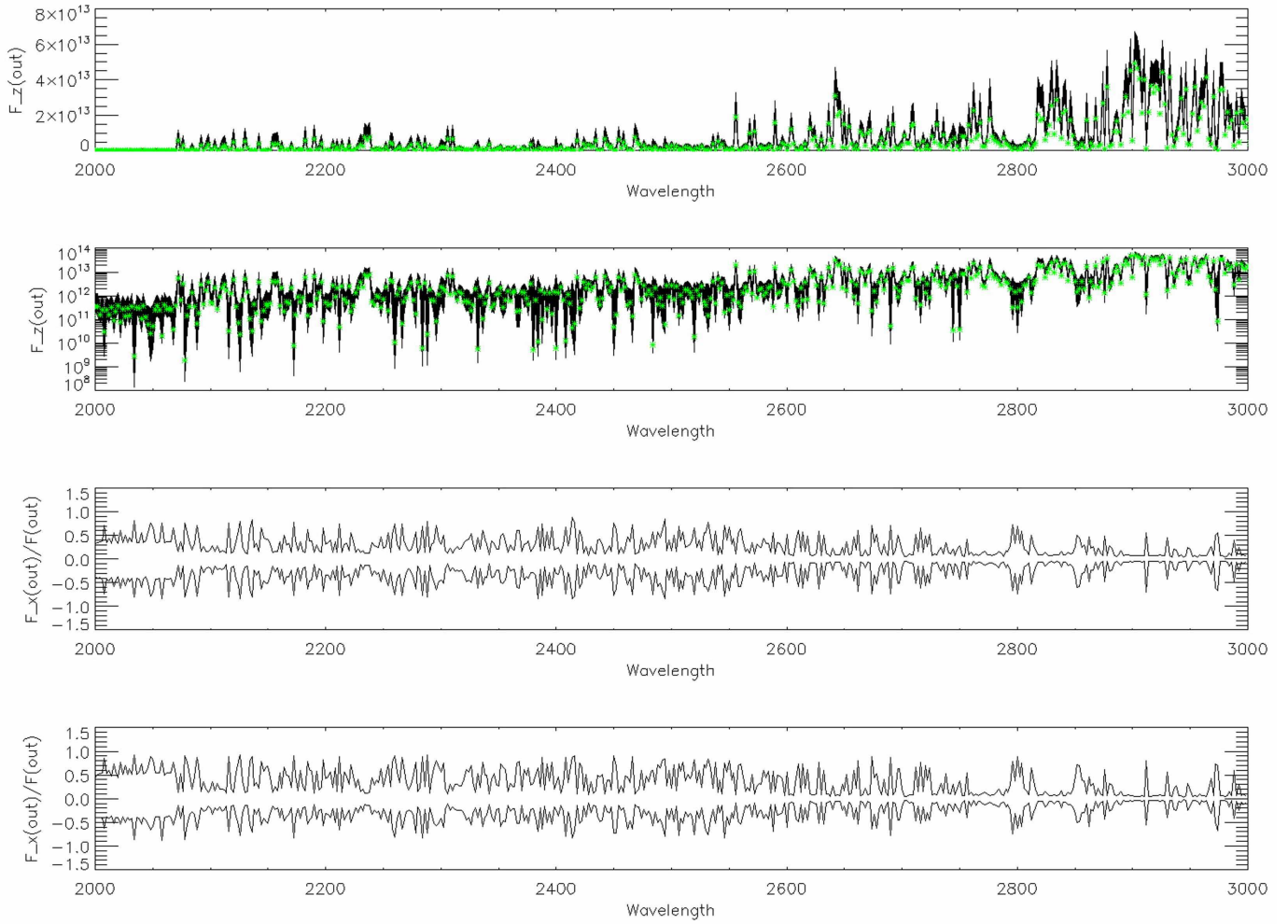


Fig. 12. Comparison between the flux vectors across the outermost voxels for the PHOENIX/3D near UV spectra computed for the 3D hydro structure and the PHOENIX/1D spectrum for the G2V dwarf test model ($T_{\text{eff}} = 5700\text{K}$, $\log(g) = 4.5$). In the PHOENIX/3D calculations we have used a 3D coordinate system with a total of $141 \times 141 \times 151$ Cartesian grid points in x , y , and z , respectively, the periodic boundary conditions are set in the (horizontal) x, y plane. The 3D radiative transport equation is solved for $n_{\theta} = 64$ and $n_{\phi} = 64$ solid angle points. The top panels show the F_z component of all outer voxels in linear and logarithmic scales, respectively, compared to the results of the 1D comparison model. The bottom panels show the corresponding maxima and minima of $F_x/|\mathbf{F}|$ and $F_y/|\mathbf{F}|$, respectively, over all surface voxels for each wavelength. Note the difference between this result and that shown in the bottom two panels of Fig. 11. See text for details. The wavelengths are given in \AA and the fluxes are in cgs units.

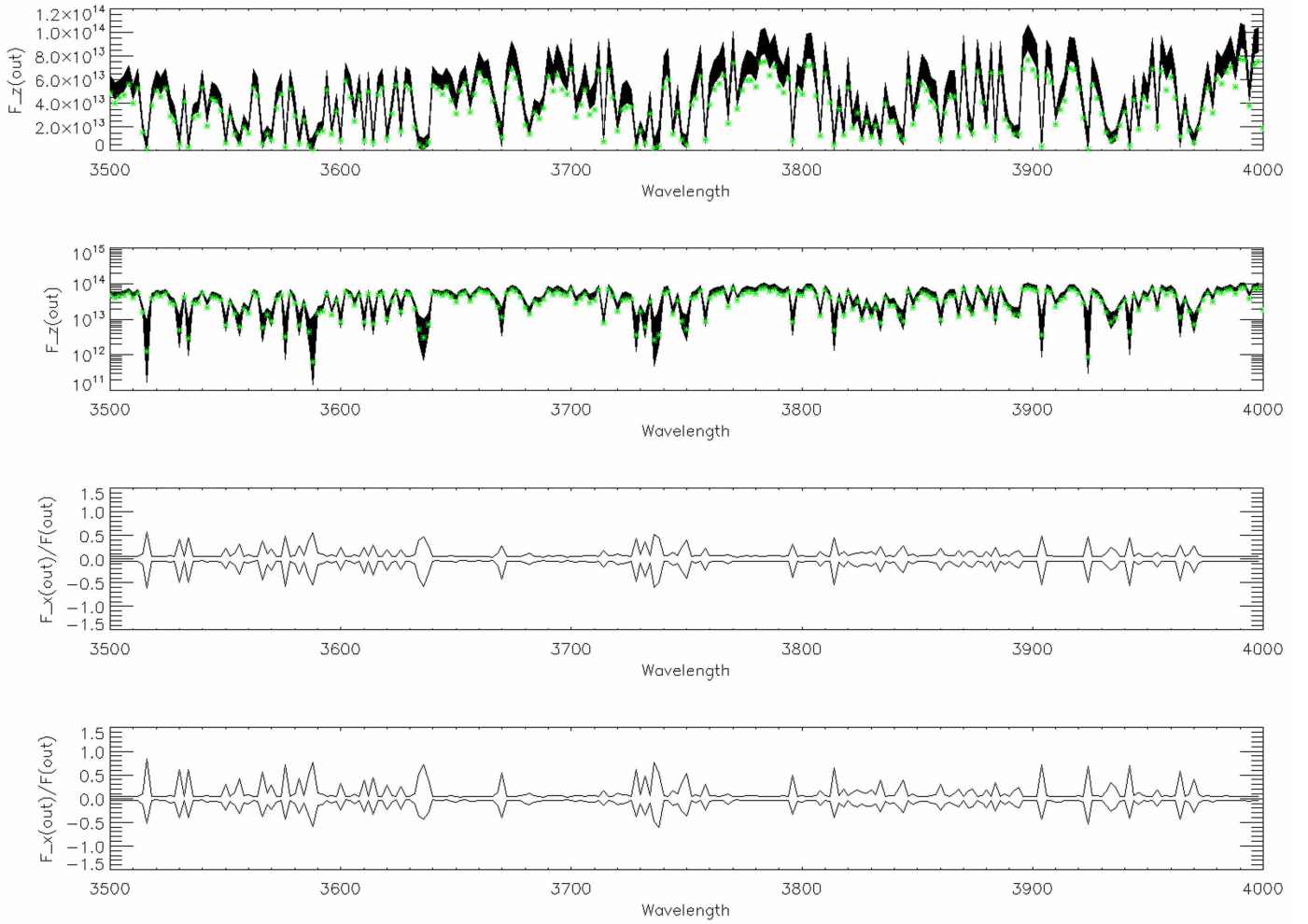


Fig. 13. Comparison between the flux vectors across the outermost voxels for the PHOENIX/3D UV spectra computed for the 3D hydro structure and the PHOENIX/1D spectrum for the G2V dwarf test model ($T_{\text{eff}} = 5700\text{K}$, $\log(g) = 4.5$). In the PHOENIX/3D calculations we have used a 3D coordinate system with a total of $141 \times 141 \times 151$ Cartesian grid points in x , y , and z , respectively, the periodic boundary conditions are set in the (horizontal) x , y plane. The 3D radiative transport equation is solved for $n_{\theta} = 64$ and $n_{\phi} = 64$ solid angle points. The top panels show the F_z component of all outer voxels in linear and logarithmic scales, respectively, compared to the results of the 1D comparison model. The bottom panels show the corresponding maxima and minima of $F_x/|F|$ and $F_y/|F|$, respectively, over all surface voxels for each wavelength. Note the difference between this result and that shown in the bottom two panels of Fig. 11. See text for details. The wavelengths are given in Å and the fluxes are in cgs units.

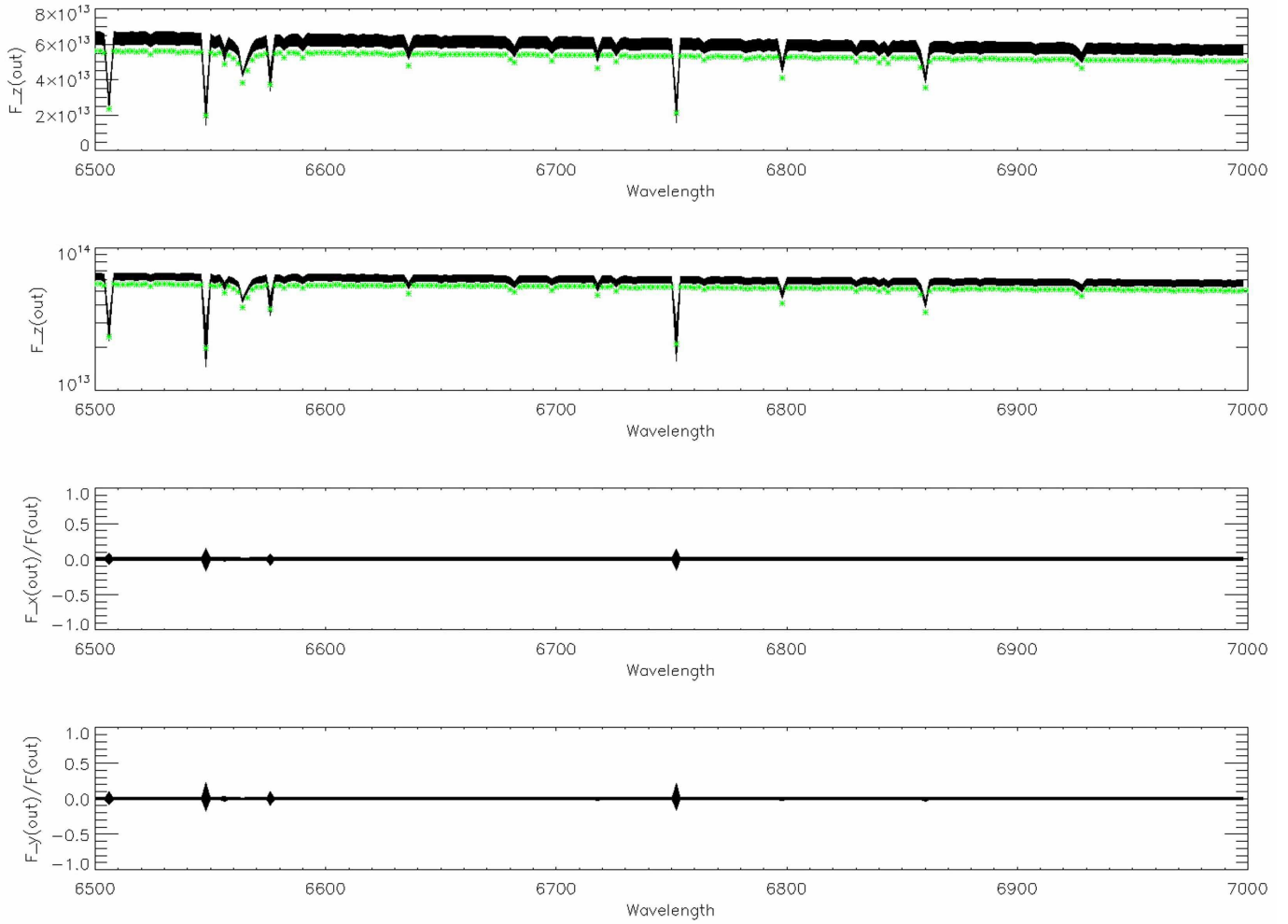


Fig. 14. Comparison between the flux vectors across the outermost voxels for the PHOENIX/3D optical spectra computed for the 3D hydro structure and the PHOENIX/1D spectrum for the G2V dwarf test model ($T_{\text{eff}} = 5700\text{K}$, $\log(g) = 4.5$). In the PHOENIX/3D calculations we have used a 3D coordinate system with a total of $141 \times 141 \times 151$ Cartesian grid points in x , y , and z , respectively, the periodic boundary conditions are set in the (horizontal) x, y plane. The 3D radiative transport equation is solved for $n_{\theta} = 64$ and $n_{\phi} = 64$ solid angle points. The top panels show the F_z component of all outer voxels in linear and logarithmic scales, respectively, compared to the results of the 1D comparison model. The bottom panels show the corresponding runs of $F_x/|\mathbf{F}|$ and $F_y/|\mathbf{F}|$, respectively. See text for details. The wavelengths are given in \AA and the fluxes are in cgs units.

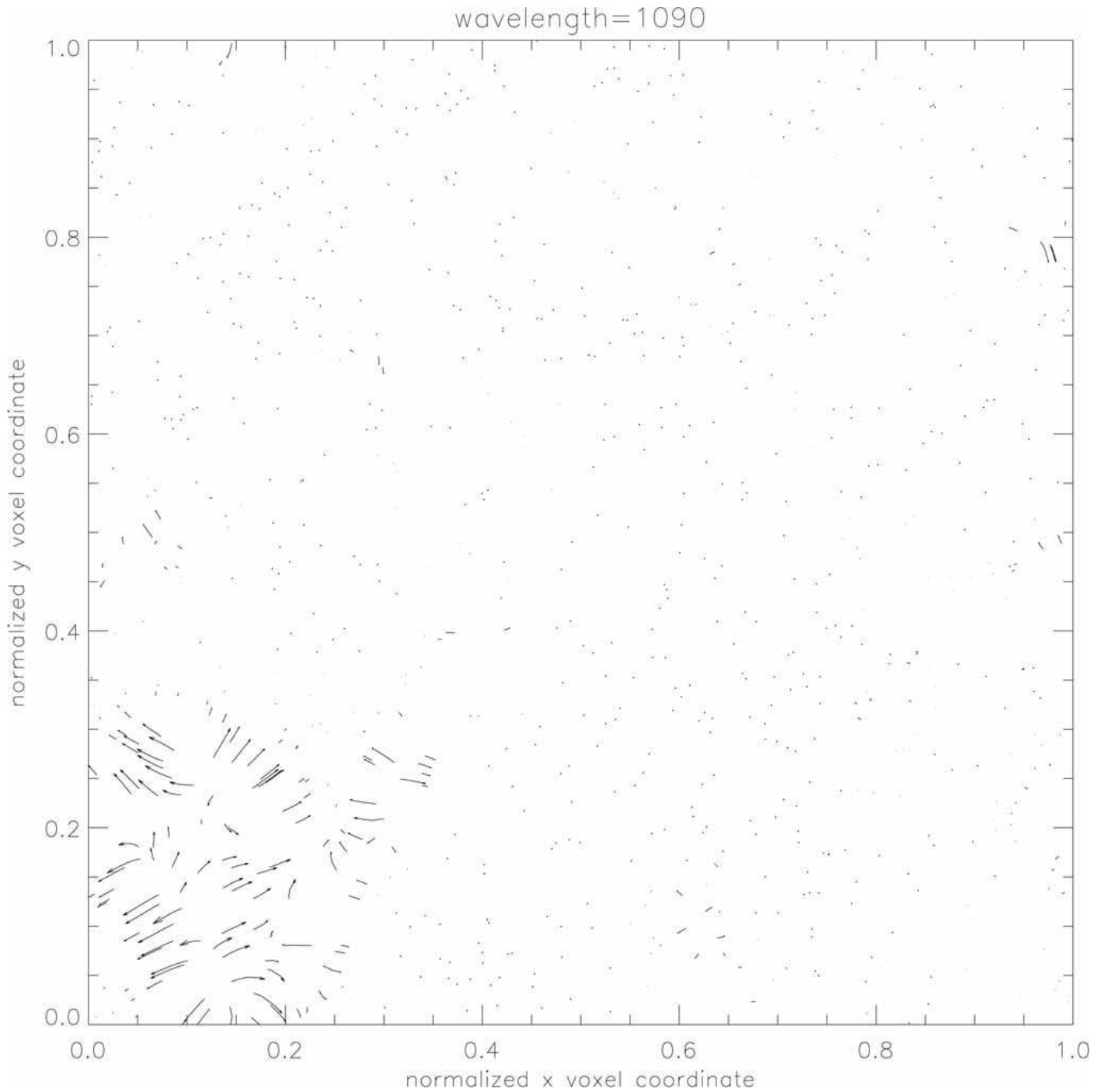


Fig. 15. Illustration of horizontal energy flow for the outermost voxels of the the 3D hydro structure for the red spectral range. The graphics shows the flowlines of the x and y components of the flux vector \mathbf{F} . Here, a flowline connects points of constant $|(F_x, F_y)|$ following the direction of (F_x, F_y) . The 3D radiative transport equation is solved for $n_\theta = 64$ and $n_\phi = 64$ solid angle points. The wavelengths are given in \AA . The normalized x and y voxel coordinates are shown on the x and y axes, respectively.

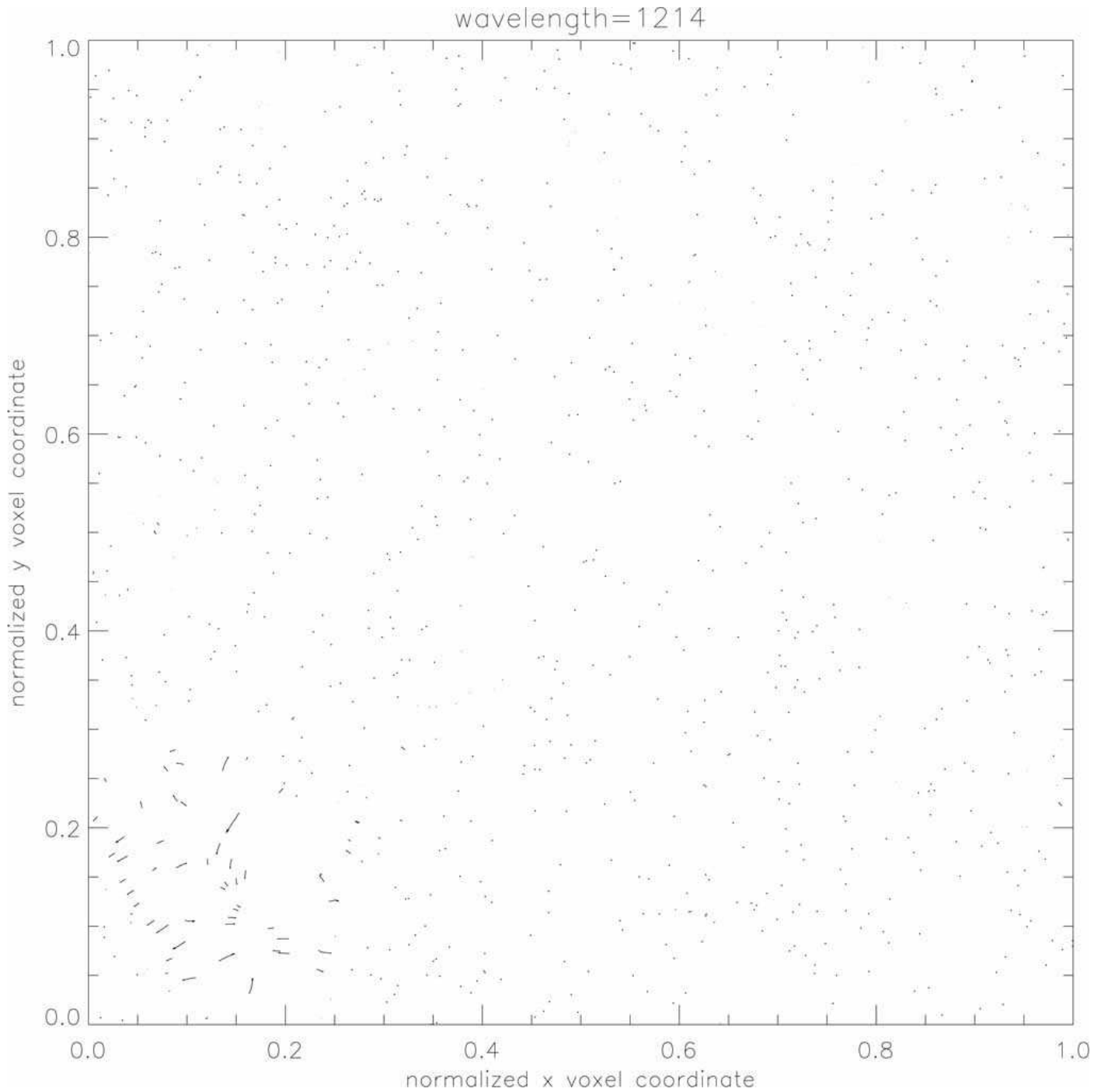


Fig. 16. Illustration of horizontal energy flow for the outermost voxels of the the 3D hydro structure for the red spectral range. The graphics shows the flowlines of the x and y components of the flux vector \mathbf{F} . Here, a flowline connects points of constant $|(F_x, F_y)|$ following the direction of (F_x, F_y) . The 3D radiative transport equation is solved for $n_\theta = 64$ and $n_\phi = 64$ solid angle points. The wavelengths are given in \AA . The normalized x and y voxel coordinates are shown on the x and y axes, respectively.

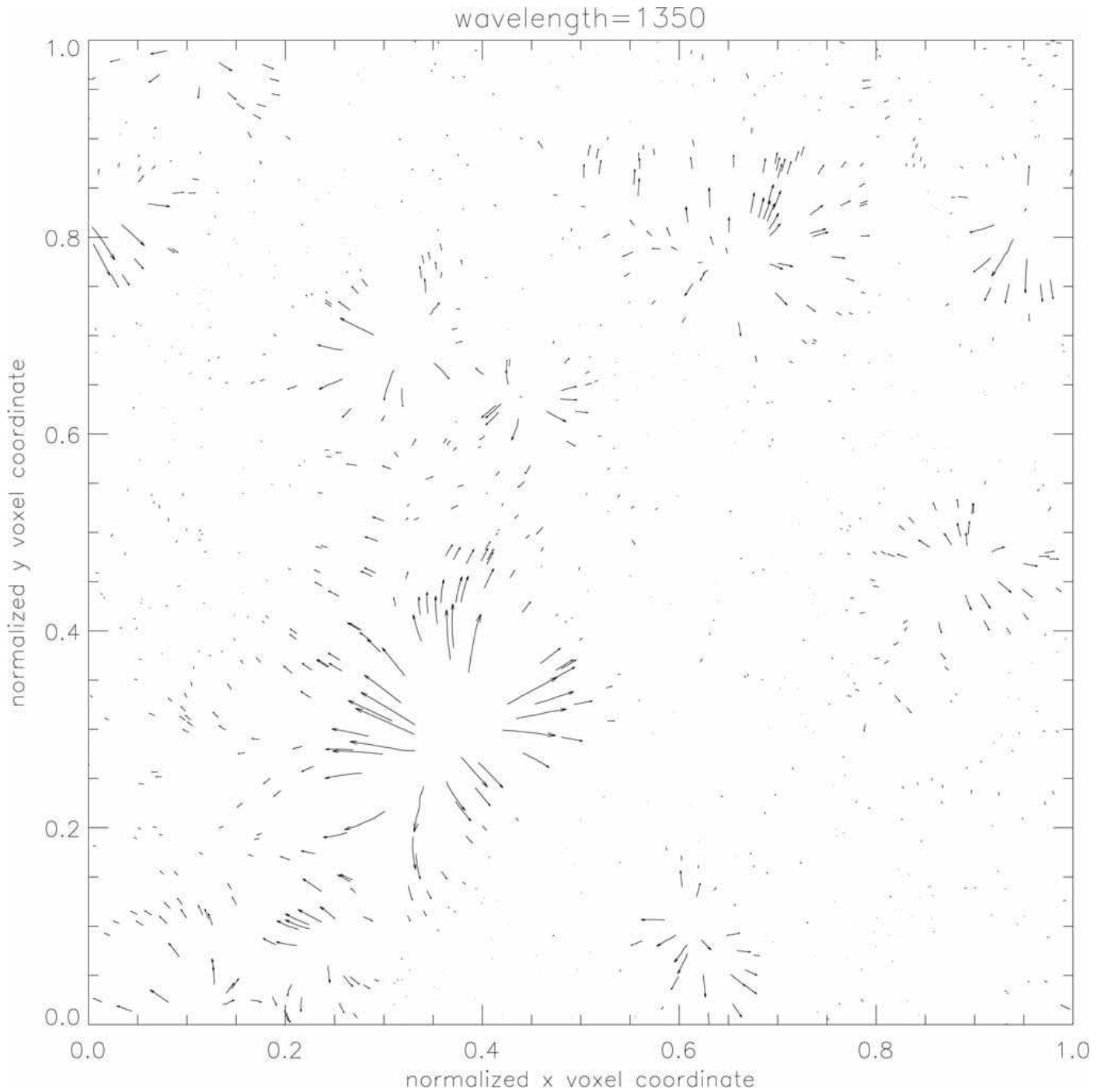


Fig. 17. Illustration of horizontal energy flow for the outermost voxels of the the 3D hydro structure for the red spectral range. The graphics shows the flowlines of the x and y components of the flux vector \mathbf{F} . Here, a flowline connects points of constant $|(F_x, F_y)|$ following the direction of (F_x, F_y) . The 3D radiative transport equation is solved for $n_\theta = 64$ and $n_\phi = 64$ solid angle points. The wavelengths are given in \AA . The normalized x and y voxel coordinates are shown on the x and y axes, respectively.

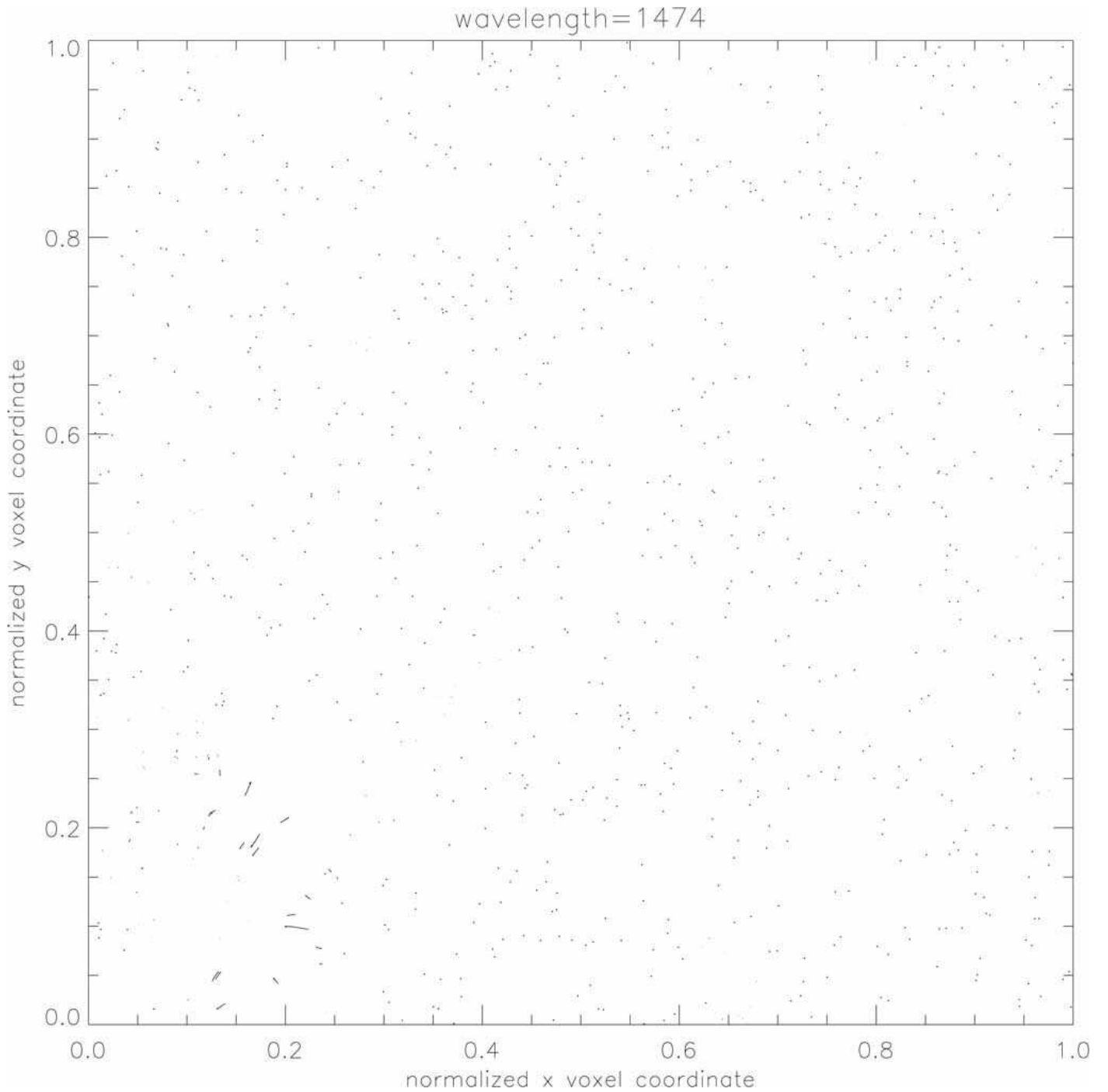


Fig. 18. Illustration of horizontal energy flow for the outermost voxels of the the 3D hydro structure for the red spectral range. The graphics shows the flowlines of the x and y components of the flux vector \mathbf{F} . Here, a flowline connects points of constant $|(F_x, F_y)|$ following the direction of (F_x, F_y) . The 3D radiative transport equation is solved for $n_\theta = 64$ and $n_\phi = 64$ solid angle points. The wavelengths are given in \AA . The normalized x and y voxel coordinates are shown on the x and y axes, respectively.

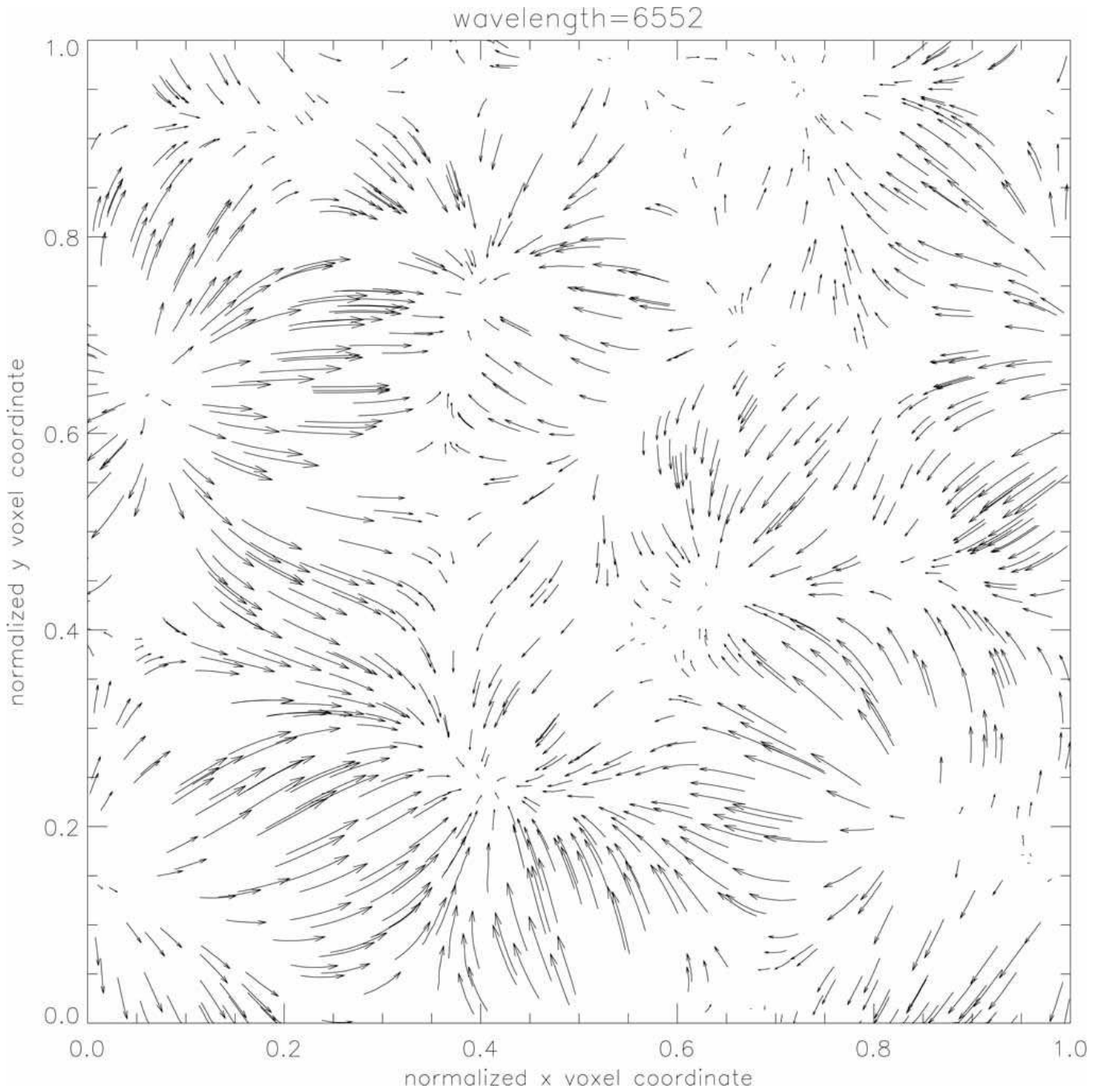


Fig. 19. Illustration of horizontal energy flow for the outermost voxels of the the 3D hydro structure for the red spectral range. The graphics shows the flowlines of the x and y components of the flux vector \mathbf{F} . Here, a flowline connects points of constant $|(F_x, F_y)|$ following the direction of (F_x, F_y) . The 3D radiative transport equation is solved for $n_\theta = 64$ and $n_\phi = 64$ solid angle points. The wavelengths are given in \AA . The normalized x and y voxel coordinates are shown on the x and y axes, respectively.

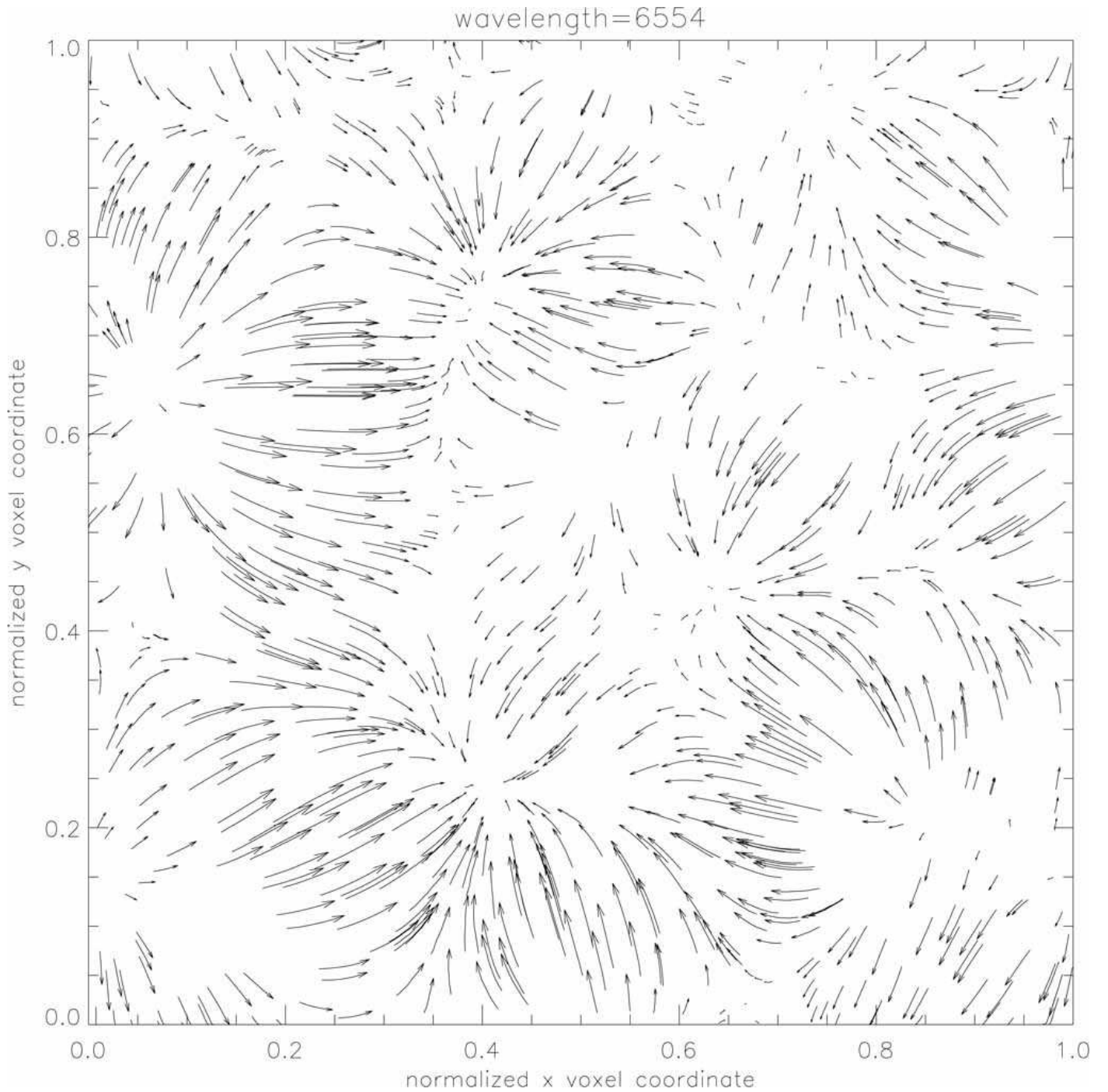


Fig. 20. Illustration of horizontal energy flow for the outermost voxels of the the 3D hydro structure for the red spectral range. The graphics shows the flowlines of the x and y components of the flux vector \mathbf{F} . Here, a flowline connects points of constant $|(F_x, F_y)|$ following the direction of (F_x, F_y) . The 3D radiative transport equation is solved for $n_\theta = 64$ and $n_\phi = 64$ solid angle points. The wavelengths are given in \AA . The normalized x and y voxel coordinates are shown on the x and y axes, respectively.

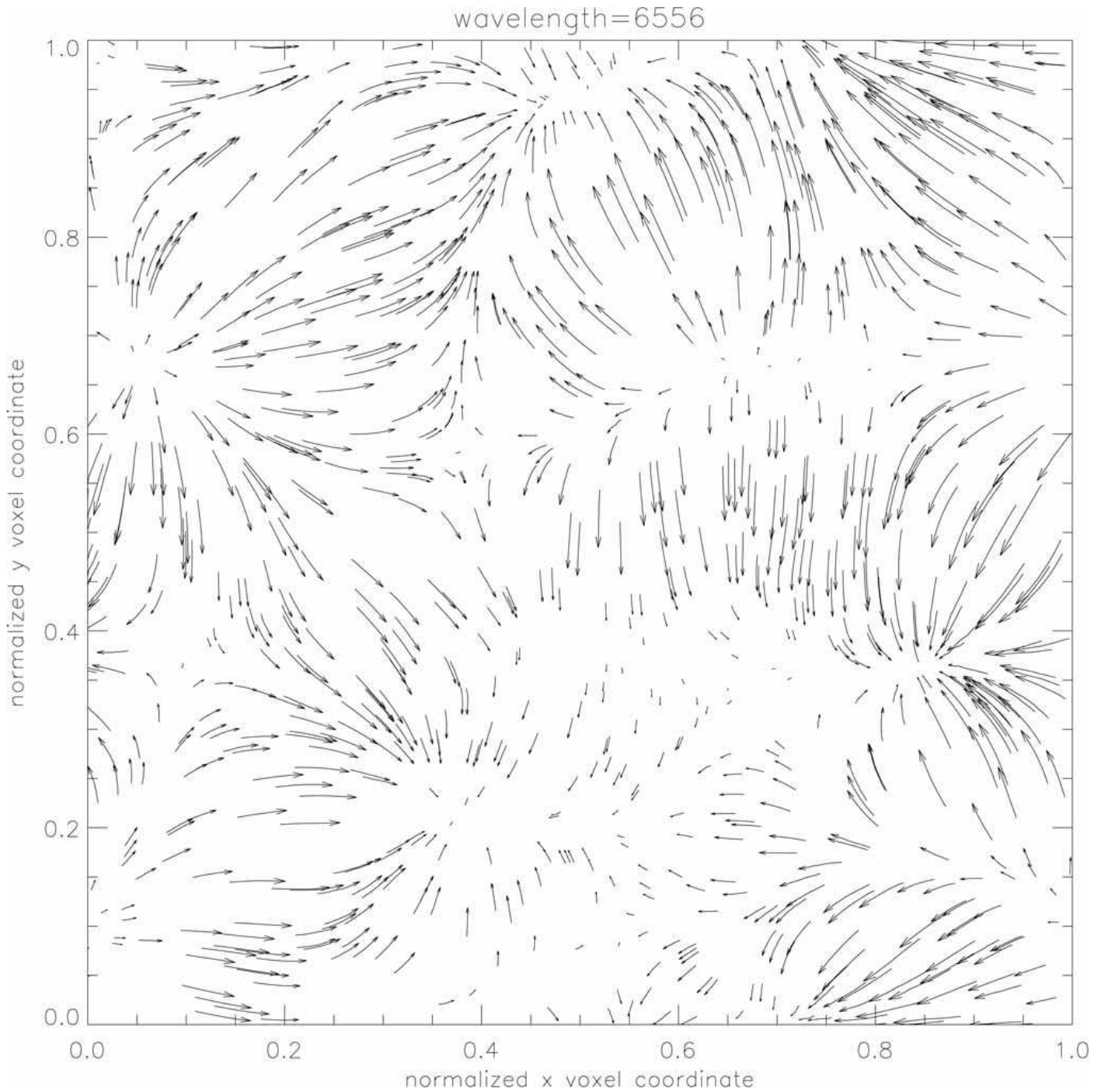


Fig. 21. Illustration of horizontal energy flow for the outermost voxels of the the 3D hydro structure for the red spectral range. The graphics shows the flowlines of the x and y components of the flux vector \mathbf{F} . Here, a flowline connects points of constant $|(F_x, F_y)|$ following the direction of (F_x, F_y) . The 3D radiative transport equation is solved for $n_\theta = 64$ and $n_\phi = 64$ solid angle points. The wavelengths are given in \AA . The normalized x and y voxel coordinates are shown on the x and y axes, respectively.

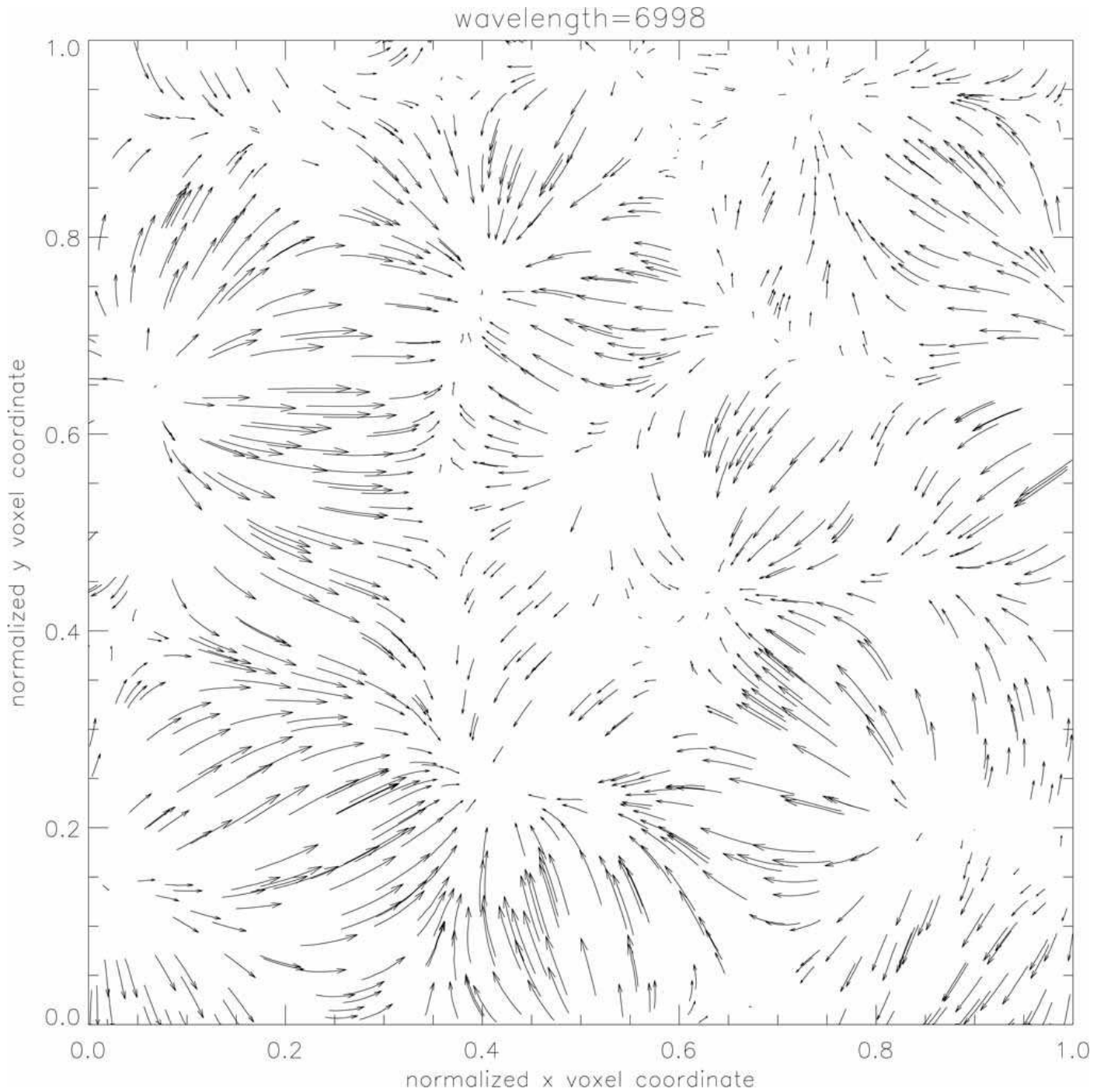


Fig. 22. Illustration of horizontal energy flow for the outermost voxels of the the 3D hydro structure for the red spectral range. The graphics shows the flowlines of the x and y components of the flux vector \mathbf{F} . Here, a flowline connects points of constant $|(F_x, F_y)|$ following the direction of (F_x, F_y) . The 3D radiative transport equation is solved for $n_\theta = 64$ and $n_\phi = 64$ solid angle points. The wavelengths are given in \AA . The normalized x and y voxel coordinates are shown on the x and y axes, respectively.

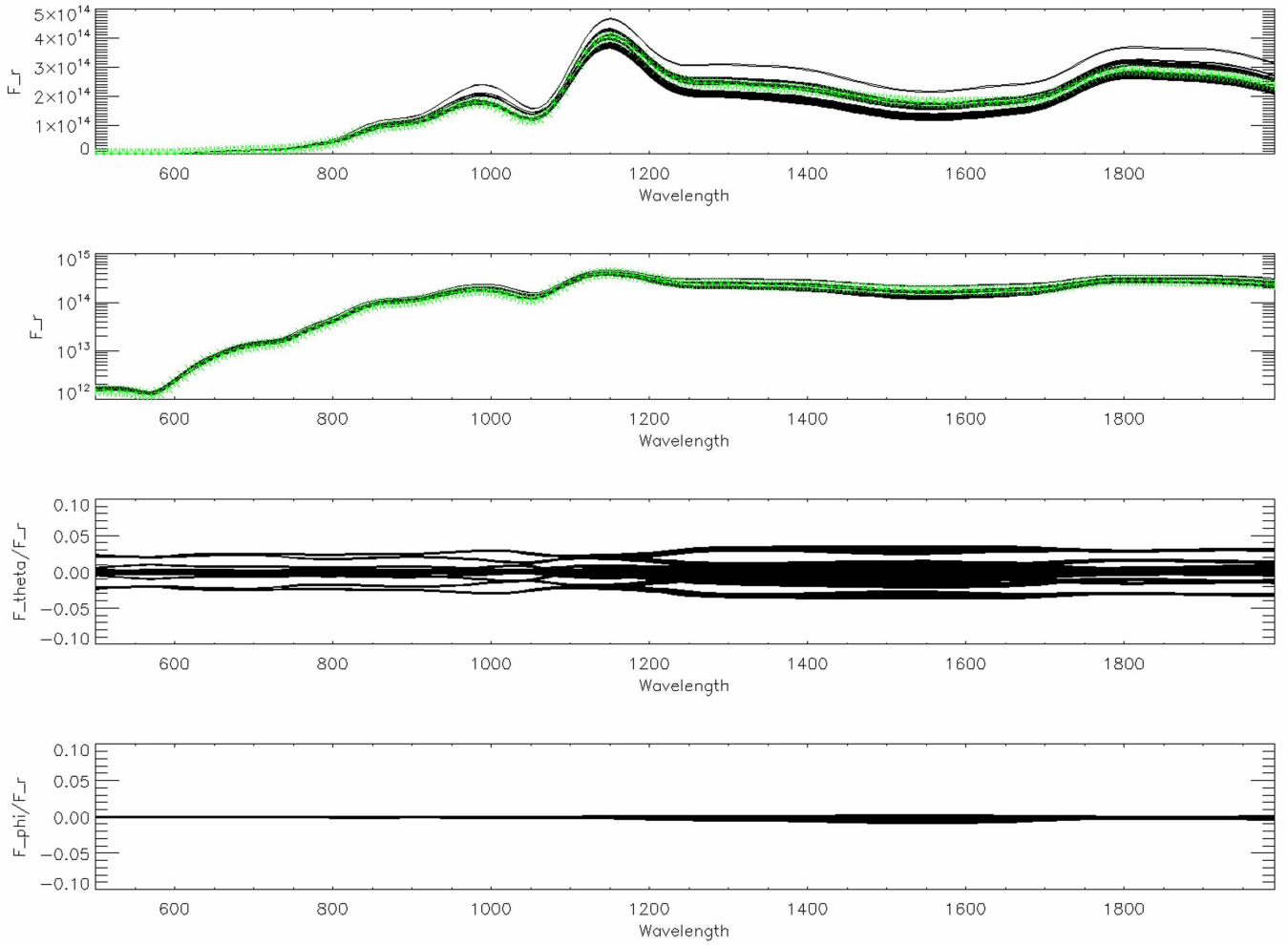


Fig. 23. Comparison between the PHOENIX/1D co-moving frame UV spectrum (computed with 256 layers, * symbols) and the co-moving frame flux vectors across the outermost voxels for the PHOENIX/3D spectra computed for the Supernova test model. In the PHOENIX/3D calculations we have used a 3D spherical coordinate system with $n_r = 129$, $n_{\theta_c} = 33$ and $n_{\phi_c} = 65$ points for a total of about 275k voxels. The calculations used 128^2 solid angle points. The top panels show the F_r component of all outer voxels in linear and logarithmic scales, respectively. The bottom panels show the corresponding runs of F_{θ}/F_r and F_{ϕ}/F_r , respectively. They should be identically zero and the deviations measure the internal accuracy. The wavelengths are given in Å and the fluxes are in cgs units.

A&A manuscript no.
(will be inserted by hand later)

Your thesaurus codes are:
missing; you have not inserted them

ASTRONOMY
AND
ASTROPHYSICS
3.11.2018

MAINTITLE should be given

Name(s) and initial(s) of author(s) should be given

Address(es) of author(s) should be given.

[the date of receipt and acceptance should be inserted later]

Abstract. Not yet given.

Key words: Not yet given.
